THE DEACTIVATION OF GAMMA-ALUMINA BASED CATALYST DURING AQUEOUS PHASE REACTION USING DENSITY FUNCTION THEORY

Miss Phakaorn Aphichoksiri

จุฬาลงกรณ์มหาวิทยาลัย
CHULALONGKORN UNIVERSITY

A Thesis Submitted in Partial Fulfillment of the Requirements
for the Degree of Master of Engineering in Chemical Engineering
Department of Chemical Engineering
FACULTY OF ENGINEERING
Chulalongkorn University
Academic Year 2020
Copyright of Chulalongkorn University

การเสื่อมของตัวเร่งปฏิกิริยาแกมมาอะลูมินาสำหรับปฏิกิริยาในวัฏภาคของเหลว โดยทฤษฎีฟังก์ชันนอลความหนาแน่น

น.ส.ภคอร อภิโชคสิริ

จุฬาลงกรณ์มหาวิทยาลัย
CHULALONGKORN UNIVERSITY

วิทยานิพนธ์นี้เป็นส่วนหนึ่งของการศึกษาตามหลักสูตรปริญญาวิศวกรรมศาสตรมหาบัณฑิต
สาขาวิชาวิศวกรรมเคมี ภาควิชาวิศวกรรมเคมี
คณะวิศวกรรมศาสตร์ จุฬาลงกรณ์มหาวิทยาลัย
ปีการศึกษา 2563

ลิขสิทธิ์ของจุฬาลงกรณ์มหาวิทยาลัย

Thesis Title	THE DEACTIVATION OF GAMMA-ALUMINA BASED CATALYST DURING AQUEOUS PHASE REACTION USING DENSITY FUNCTION THEORY
By	Miss Phakaorn Aphichoksiri
Field of Study	Chemical Engineering
Thesis Advisor	Assistant Professor SUPAREAK PRASERTHDAM, Ph.D.
Thesis Co Advisor	Tinnakorn Saelee, Ph.D.

Accepted by the FACULTY OF ENGINEERING, Chulalongkorn University in Partial Fulfillment of the Requirement for the Master of Engineering

..... Dean of the FACULTY OF ENGINEERING
(Professor SUPOT TEACHAVORASINSKUN, Ph.D.)

THESIS COMMITTEE

..... Chairman
(CHUTIMON SATIRAPIPATHKUL, Ph.D.)

..... Thesis Advisor
(Assistant Professor SUPAREAK PRASERTHDAM, Ph.D.)

..... Thesis Co-Advisor
(Tinnakorn Saelee, Ph.D.)

..... Examiner
(KRITCHART WONGWAILIKHIT, Ph.D.)

..... External Examiner
(Anchalee Junkaew, Ph.D.)

จุฬาลงกรณ์มหาวิทยาลัย
CHULALONGKORN UNIVERSITY

ภคอร อภิโชคสิริ : การเสื่อมของตัวเร่งปฏิกิริยาแกมมาอะลูมินาสำหรับปฏิกิริยาในวัฏภาคของเหลว โดยทฤษฎีฟังก์ชันนอลความหนาแน่น. (THE DEACTIVATION OF GAMMA-ALUMINA BASED CATALYST DURING AQUEOUS PHASE REACTION USING DENSITY FUNCTION THEORY) อ.ที่ปรึกษาหลัก : ผศ. ดร.ศุภฤกษ์ ประเสริฐธรรม, อ.ที่ปรึกษาร่วม : ดร.ทินกร แซ่หลี

กระบวนการแปลงสภาพชีวมวล เป็นกระบวนการที่สำคัญในการผลิตเชื้อเพลิงและสารเคมีมูลค่าสูงจากชีวมวลผ่านปฏิกิริยาต่างๆ แกมมาอะลูมินาถูกนำมาใช้ในปฏิกิริยาที่เกี่ยวข้องกับการแปลงสภาพชีวมวล โดยเฉพาะกระบวนการที่ดำเนินปฏิกิริยาในวัฏภาคของเหลวที่มีน้ำเป็นองค์ประกอบ การเกิดโค้กเป็นสาเหตุสำคัญที่ทำให้เกิดการเสื่อมสภาพของแกมมาอะลูมินาในปฏิกิริยาเคมีความร้อน และการดำเนินปฏิกิริยาในของเหลวที่มีน้ำเป็นองค์ประกอบทำให้เกิดปฏิกิริยาไฮดรอกซิเลชันบนแกมมาอะลูมินาจนกระทั่งแกมมาอะลูมินาเกิดการเปลี่ยนเฟส โดยการเปลี่ยนเฟสของแกมมาอะลูมินาเป็นสาเหตุหนึ่งของการเสื่อมของตัวเร่งปฏิกิริยา นอกจากนี้การเกิดออกซิเจนวาแคนซีอาจจะมีผลต่อการเสื่อมของแกมมาอะลูมินา งานวิจัยนี้มีวัตถุประสงค์เพื่อศึกษาความสัมพันธ์ของการเกิดโค้ก การเปลี่ยนแปลงเฟส และการเกิดออกซิเจนวาแคนซีบนแกมมาอะลูมินาโดยใช้ทฤษฎีฟังก์ชันนอลความหนาแน่น ในส่วนแรกของงานวิจัยเป็นการศึกษาการก่อตัวของโค้กบนแกมมาอะลูมินา โดยใช้แบบจำลอง γ-Al_2O_3 (110) เป็นตัวแทนของแกมมาอะลูมินา พบว่าโค้กจะเกิดการดูดซับเชิงเคมีบนพื้นผิว γ-Al_2O_3 (110) และเมื่อเกิดการสะสมโค้กบนพื้นผิว พบว่ามีโค้กที่เกิดขึ้นจะมีลักษณะแบบวงมากกว่าแบบสายโซ่ เมื่อศึกษาความสัมพันธ์ระหว่างการเกิดของโค้กและการเปลี่ยนเฟสของแกมมาอะลูมินาเนื่องจากการเกิดปฏิกิริยาไฮดรอกซิเลชันบนแกมมาอะลูมินา โดยใช้แบบจำลอง OH/γ-Al_2O_3 (110) เป็นตัวแทนพื้นผิวแกมมาอะลูมินาที่เกิดไฮดรอกซิเลชันด้วยโมเลกุลของน้ำบางส่วน และแบบจำลอง γ-AlOOH(010) เป็นตัวแทนของพื้นผิวที่เกิดไฮดรอกซิเลชันอย่างสมบูรณ์จนเกิดการเปลี่ยนแปลงเฟส จากผลการศึกษาพบว่า การเกิดไฮดรอกซิเลชันบนแกมมาอะลูมินาจะส่งผลให้อันตรกิริยาระหว่างโค้กกับพื้นผิวลดลง ในขณะที่การสะสมของโค้กบนแกมมาอะลูมินาจะเกิดได้ดีขึ้นเมื่อเกิดไฮดรอกซิเลชันบนแกมมาอะลูมินา เมื่อศึกษาความสัมพันธ์ระหว่างการเกิดโค้ก และการเกิดออกซิเจนวาแคนซี โดยใช้แบบจำลอง Ov/OH/γ-Al_2O_3 (110) เป็นตัวแทนพื้นผิวเกิดออกซิเจนวาแคนซีในวัฏภาคของเหลว จากการศึกษาพบว่า ออกซิเจนวาแคนซีทำให้อันตรกิริยาระหว่างโค้กกับพื้นผิวเพิ่มขึ้น และส่งเสริมการเกิดโค้กบนพื้นผิวของแกมมาอะลูมินา ทำให้การกำจัดโค้กยากขึ้น นอกจากนี้เมื่อพิจาณาผลของอุณหภูมิ (373-773 K) การอุณหภูมิเพิ่มขึ้นจะส่งผลทำให้ให้อันตรกิริยาระหว่างโค้กกับพื้นผิวลดลง ส่วนสุดท้ายศึกษาความเป็นไปได้เป็นการเกิดการสะสมโค้กบนแกมมาอะลูมินาจากการเกิดโค้กไดเมอร์ไรเซชัน เมื่อพิจารณาค่าพลังงานอิสระกิบส์พบว่าปฏิกิริยาโค้กไดเมอร์ไรเซชันเป็นปฏิกิริยาที่สามารถเกิดขึ้นได้เอง และมีพลังงานขั้นต่ำในการเกิดปฏิกิริยาเท่ากับ 1.89 อิเล็กตรอนโวลต์

สาขาวิชา	วิศวกรรมเคมี	ลายมือชื่อนิสิต .....
ปีการศึกษา	2563	ลายมือชื่อ อ.ที่ปรึกษาหลัก .....
		ลายมือชื่อ อ.ที่ปรึกษาร่วม .....

CHULALONGKORN UNIVERSITY

6270200021 : MAJOR CHEMICAL ENGINEERING
KEYWORD: γ-Al2O3, catalyst deactivation, density functional theory (DFT)

Phakaorn Aphichoksiri : THE DEACTIVATION OF GAMMA-ALUMINA BASED CATALYST DURING AQUEOUS PHASE REACTION USING DENSITY FUNCTION THEORY. Advisor: Asst. Prof. SUPAREAK PRASERTHDAM, Ph.D. Co-advisor: Tinnakorn Saelee, Ph.D.

Nowadays, biomass conversion has become a more attractive process to produce fuels and various high-value chemicals from biological materials. From many kinds of catalysts, the metal-supported gamma-alumina (γ-Al_2O_3) is a widely used catalyst for various transformation processes, especially in the aqueous phase reaction. Typically, coke formation on γ-Al_2O_3 causes catalyst deactivation in the thermal reaction process. Moreover, incorporation of aqueous phase medium initiates hydroxylation of γ-Al_2O_3 and phase transformation of γ-AlOOH, leading to the catalyst deactivation. Not only coke formation and phase transformation are the cause of catalytic deactivation, but the oxygen vacancy, changing the activity of the catalyst, should also be the cause of the deactivation of γ-Al_2O_3. To understand the interplay between coke formation, oxygen vacancy, and phase transformation, the coke formation on the γ-Al_2O_3 catalyst has been theoretically investigated using density functional theory (DFT). Starting with the coke formation on the γ-Al_2O_3 surface, the coke is strongly chemisorbed, and the forming higher coke prefers a cyclic form to the aliphatic on the γ-Al_2O_3 surface. Afterward, the effects of partial hydroxylation on γ-Al_2O_3 forming OH/γ-Al_2O_3 and full hydroxylation until phase transformation forming γ-AlOOH on coke formation were also investigated. Hydroxylation of the γ-Al_2O_3 surface can suppress the interaction between coke and the surface. However, the covered surface with the hydroxyl group promotes coke polymerization, as evidenced by the relative formation energy. In addition, the effect of oxygen vacancy on coke formation was investigated. The presence of oxygen vacancy has a remarkable impact on the coke formation and makes the elimination more difficult. Moreover, the thermal effect was also investigated at 373 to 773 K. The increasing temperature diminishes the adsorption strength, leading to the weak interaction between coke and the surface. Finally, the coke dimerization has been explored to predict the feasibility of coke evolution on the γ-Al_2O_3, demonstrating that the dimerization is spontaneous and can occur with the energy barrier of 1.89 eV.

Field of Study:	Chemical Engineering	Student's Signature .....
Academic Year:	2020	Advisor's Signature .....
		Co-advisor's Signature .....

ACKNOWLEDGEMENTS

Firstly, I would like to thank funding from (1) the Faculty of Engineering, Chulalongkorn University, and (2) the Center of Excellence on Catalysis and Catalytic Reaction Engineering (CECC), Chemical Engineering, Faculty of Engineering, Chulalongkorn University.

I am extremely grateful to my advisor and co-advisor, Asst. Prof. Supareak Praserthdam and Dr. Tinnakorn Saelee for their invaluable advice and guidance throughout the research. I would also like to thank Dr. Meena Rittiruam for his help and treasured support. In addition, I would like to thank my committee members Dr. Chutimon Satirapipatkul, Dr. Kritchart Wongwailikhit, and Dr. Anchalee Junkaew, for providing suggestions. Finally, I would like to special thanks to parents and friends for their continued support and encouragement.

Phakaorn Aphichoksiri

จุฬาลงกรณ์มหาวิทยาลัย
CHULALONGKORN UNIVERSITY

TABLE OF CONTENTS

Page

..... iii

ABSTRACT (THAI) iii

.....iv

ABSTRACT (ENGLISH).....iv

ACKNOWLEDGEMENTS.....v

TABLE OF CONTENTS.....vi

LIST OF TABLES..... viii

LIST OF FIGURES ix

CHAPTER 1 INTRODUCTION 1

1.1 Introduction.....1

1.2 Objective.....3

1.3 The scope of the research 3

1.4 Research Methodology 4

CHAPTER 2 BACKGROUND AND LITERATURE REVIEWS 5

2.1 Density Functional Theory (DFT) 5

2.1.1 Kohn-Sham equation.....6

2.1.2 Exchange correlation approximation.....7

2.2.3 Periodic boundary conditions (PBC).....8

2.2.4 Plane wave based DFT method 8

2.2 Biomass conversion in the aqueous phase.....9

2.3 Deactivation on Alumina in the aqueous phase.....1

2.4 Coking.....2

2.5 Phase transformation 5

2.6 Oxygen vacancy.....6

2.7 Literature reviews 6

CHAPTER 3 COMPUTATIONAL DETAILS AND METHODOLOGY.....10
3.1 Computational methods and parameter 10
3.2 Structure Model 11
3.2.1 The γ-Al_2O_3 surface 11
3.2.2 The OH/ γ-Al_2O_3 surface.....12
3.2.3 The γ-AlOOH surface.....13
3.2.4 The isolated-coke molecule.....14
CHAPTER 4 RESULTS AND DISCUSSIONS.....15
4.1 Coke behavior on γ-Al_2O_3 15
4.1.1 Coke adsorption on γ-Al_2O_3.....15
4.1.2 Coke evolution on γ-Al_2O_3.....17
4.1.3 Feasibility of coke evolution 20
4.2 Effect of water coverage on coke behaviour 22
4.2.1 Coke adsorption on the partial and fully hydroxylated surface.....23
4.2.2 Coke evolution on the partial and fully hydroxylated surface 24
4.2.3 The Electronic properties 26
4.3 Effect of oxygen vacancy on coke behavior.....29
4.3.1 Coke adsorption on the oxygen vacancy surface 29
4.3.2 Coke evolution on the oxygen vacancy surface 31
4.3.2 The Electronic properties 32
4.4 Effect of temperature 34
CHAPTER 5 CONCLUSION.....35
REFERENCES 37
VITA 42

LIST OF TABLES

Page

Table 1 The general types of deactivation in liquid media. 1

Table 2 Adsorption energy and bond distance of coke adsorption on γ-Al_2O_3 (110) surface. 16

Table 3 The formation energy of coke on γ-Al_2O_3 (110) surface. 20

Table 4 Adsorption energy of various types of coke on the γ-Al_2O_3 (110), OH/γ-Al_2O_3 (110), and γ-AlOOH (010) surface. 24

Table 5 The relative ΔE_{form} of coke evolution along the γ-Al_2O_3 (110), OH/γ-Al_2O_3 (110), and γ-AlOOH (010) surface. 25

Table 6 Bader charge change of each component for coke adsorption on γ-Al_2O_3, OH/ γ-Al_2O_3, and γ-AlOOH surface. 28

Table 7 Adsorption energy of coke adsorption on OH/ γ-Al_2O_3 and O_v/OH/ γ-Al_2O_3 surface. 30

Table 8 The relative formation energy of coke on OH/γ-Al_2O_3 (110), and O_v/OH/γ-Al_2O_3 surface. 31

Table 9 The Bader charge change of each component for coke adsorption on OH/γ-Al_2O_3 (110) and O_v/OH/γ-Al_2O_3 (110) surface. 33

จุฬาลงกรณ์มหาวิทยาลัย
CHULALONGKORN UNIVERSITY

LIST OF FIGURES

Page

Figure 1 Scope of the research 3

Figure 2 Research Methodology 4

Figure 3 Periodic boundary conditions. 8

Figure 4 Transformation of carbohydrate-based feedstocks to fuels and chemicals. ... 1

Figure 5 The characteristic of coke deposited on catalyst in reforming reactions 3

Figure 6 The coke formation mechanism on metal oxide and sulfide catalysts 5

Figure 7 The space group of boehmite 9

Figure 8 Surface model for γ-Al_2O_3 (110) 12

Figure 9 Surface model for OH/γ-Al_2O_3 (110). 13

Figure 10 Surface model for γ-AlOOH (010) 14

Figure 11 The various types of molecules used in coke adsorption. 14

Figure 12 The most stable configuration of coke on γ-Al_2O_3 (110) surface in the initial stage 16

Figure 13 The most stable configuration of coke adsorption on the γ-Al_2O_3 surface in the polymerization stage 17

Figure 14 Proposed mechanism of coke evolution through the continuous growth ... 18

Figure 15 The relative ΔE_{form} diagram for the coke evolution on γ-Al_2O_3 (110) surface 20

Figure 16 The coke dimerization path on the γ-Al_2O_3 surface 22

Figure 17 The most stable configuration of coke C_1-atomic, C_2-dimer, and C_6-cyclic on γ-Al_2O_3 (110), OH/γ-Al_2O_3 (110), and γ-AlOOH (010). 24

Figure 18 The relative ΔE_{form} diagram for the coke evolution on γ-Al_2O_3, OH/γ-Al_2O_3, and γ-AlOOH surface based on the LH mechanism. 26

Figure 19 Charge density differences of coke adsorption on (a) the γ-Al_2O_3, (b) the OH/ γ-Al_2O_3, and (c) the γ-AlOOH surface 28

Figure 20 The most stable configuration of the O_v/ OH/ γ-Al_2O_3 surface 29

Figure 21 The favorable adsorption of C_1-atomic, C_2-dimer, and C_6-cyclic on OH/γ-Al_2O_3 (110) and O_v/OH/ γ-Al_2O_3 (110). 30

Figure 22 The relative ΔE_{form} diagram for the coke evolution on the OH/γ-Al_2O_3 (110) and O_v/OH/γ-Al_2O_3 (110) surface based on LH mechanism 32

Figure 23 Charge density differences of coke adsorption on (a) OH/γ-Al_2O_3 and (b) O_v/OH/γ-Al_2O_3 surface 33

Figure 24 The ΔGads profiles of γ-Al_2O_3(110), OH/γ-Al_2O_3(110), γ-AlOOH(010), and Ov/OH/γ-Al_2O_3(110) surface in the temperatures of 373 - 773 K 34

จุฬาลงกรณ์มหาวิทยาลัย
CHULALONGKORN UNIVERSITY

CHAPTER 1

INTRODUCTION

1.1 Introduction

Global energy demand is dramatically increased, whereas the scarcity of conventional resources, petroleum fuel, and environmental impact is a concern. Therefore, an energy assessment trend is changed direction to the alternative resources that are cleaner and more sustainable. According to these reasons, biomass is a remarkable resource, especially lignocellulose, presented as a promising source because of abundant and non-competitor food production. Lignocellulose composes of cellulose as the main component.

Biomass conversion is the potential process to produce fuels and various high-value chemicals through the transformation routes for the beneficial use of lignocellulose. Glucose, a monomer unit from cellulose hydrolysis, is used as a primary platform molecule to further transformations such as dehydration, oxidation, hydrogenolysis, and reforming. Among several catalysts, the metal-supported on gamma-alumina (γ-Al_2O_3) is a widely used catalyst for various transformation routes in the aqueous phase[1,2], such as aqueous phase reforming of polyols[1,3,4], hydrogenation of levulinic acid [5] and aldol-condensation [6].

Even though there are several advantages in metal-supported γ-Al_2O_3 for aqueous phase reaction, carrying out in aqueous phase results in modifying the surface properties of γ-Al_2O_3 affected catalyst performance[7-10]. Consequently, the stability of catalyst support in the aqueous phase is crucial for catalyst improvement. In liquid media, the catalyst deactivation is classified into six types: fouling/coking, mechanical alterations, sintering, poisoning, the formation of inactive phases, and leaching[11]. However, the possible deactivation causes of γ-Al_2O_3 are irreversible phase transformation and coke formation reported in the previous study[9,12,13].

First, the irreversible phase transformation of γ-Al_2O_3 into boehmite(γ-AlOOH), which is inevitable in the aqueous phase, is one of the deactivation causes. The activity or selectivity is decreased due to the boehmite phase is less active compared to γ-Al_2O_3. For example, the transformation of γ-Al_2O_3 into boehmite and amorphous aluminum trihydroxide occurred during epoxidation using aqueous 70% H_2O_2, and the active site

was also decreased, leading to catalyst deactivation eventually. For this reason, the challenge of the stability of γ-Al_2O_3 in the aqueous phase has been gained attention [9,14]. Second, Coke deposition deactivates the catalyst by blocking active sites or pores. M. Argyle and C. Bartholomew summarized the coke formation in metal oxide and sulfide surface that involved three primary reactions: (i) polymerization of alkene, (ii) cyclization to aromatic structure, and (iii) polyaromatic formation. Besides, the coke initiation and its change were studied on the Mo/γ-Al_2O_3 with increasing time on steam during hydrotreating of Kuwaiti atmospheric residue. The tetrahydrofuran(THF) extraction shows that the aliphatic and aromatic cokes were formed during the reaction. These cokes also shifted towards increased aromatic proportion when the times on steam are increased, which is in agreement with the preferable structure that summarized in the Bartholomew's review[15]. Furthermore, defects in the structure, especially oxygen vacancy, can change the metal oxide properties [16,17]. For this reason, it is crucial to reveal the role of oxygen vacancy on the catalytic deactivation of γ-Al_2O_3.

Density functional theory (DFT) has become a powerful tool for investigating the electronic properties of the catalyst, the reaction pathway that identifies the elementary step and describes the evidence during the reaction. For example, E. J. Peterson et al.[18] proposed CO oxidation reaction mechanism on Pd/ γ-Al_2O_3 (100) based on DFT investigation. In addition, the structure-property relationship of a complex system can be separately considered at an atomic level. In the combination of several aspects, it is possible to rational design a new catalyst.

Despite several studies regarding the deactivation of γ-Al_2O_3, the effect between these causes remains unclear and could have unexpected results. In this work, the interplay between coke formation, oxygen vacancy, and phase transformation that affects the deactivation of γ-Al_2O_3 catalysts has been investigated.

1.2 Objective

To study the deactivation of γ-Al_2O_3 caused by the interplay between coke formation, phase transformation, and oxygen vacancy during aqueous phase reactions using density functional theory (DFT)

1.3 The scope of the research

1. Investigate the atomic coke initiation and graphitic coke formation on hydroxylated gamma-alumina (γ-Al_2O_3) (110) and boehmite (γ-AlOOH) (010) surfaces.
2. Study the atomic coke initiation and graphitic coke formation on defected surface (oxygen-vacancy) of hydroxylated gamma-alumina (γ-Al_2O_3) (110) surfaces.

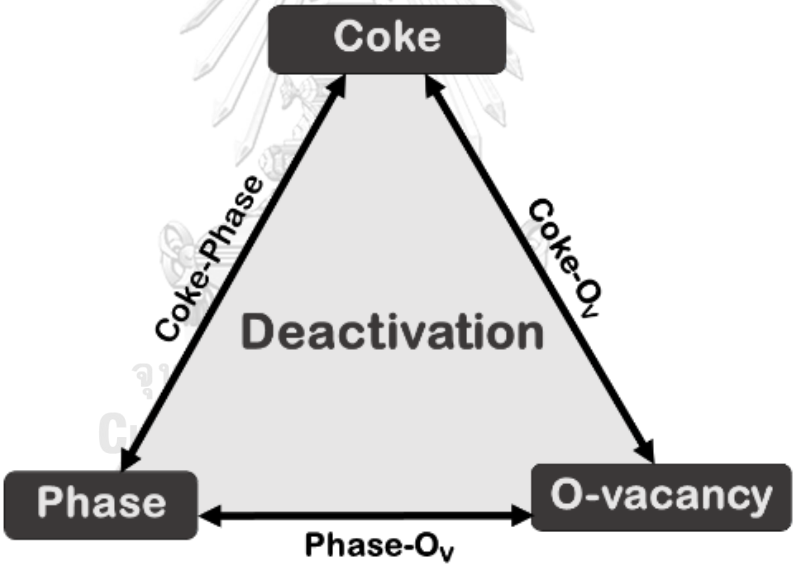

Figure 1 Scope of the research

1.4 Research Methodology

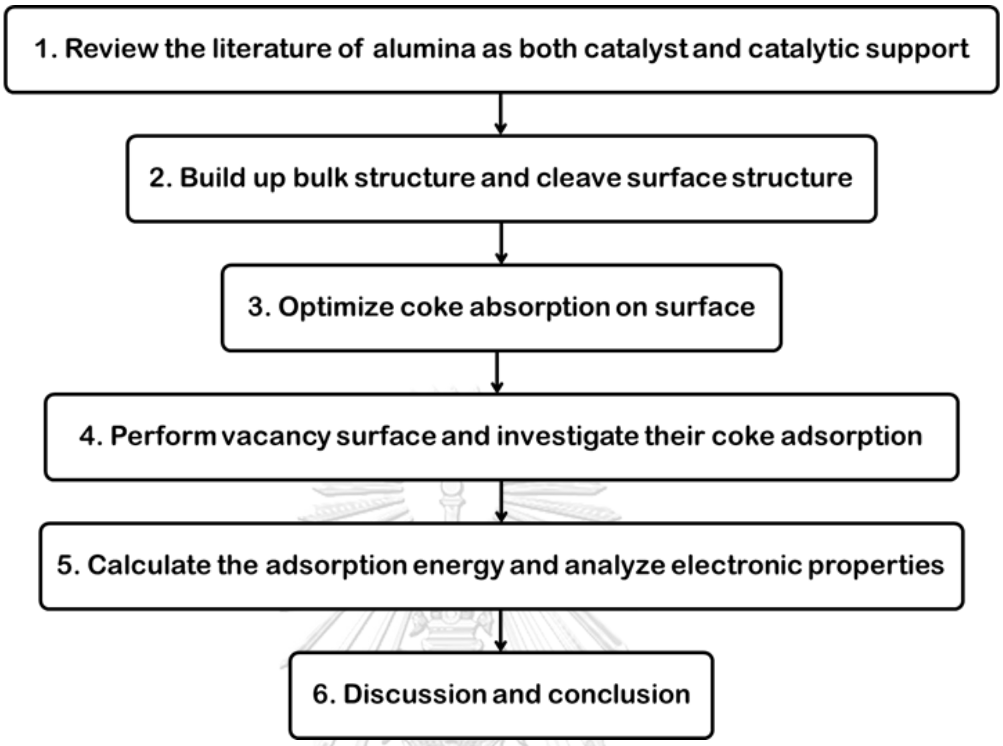

Figure 2 Research Methodology

จุฬาลงกรณ์มหาวิทยาลัย
CHULALONGKORN UNIVERSITY

CHAPTER 2
BACKGROUND AND LITERATURE REVIEWS

2.1 Density Functional Theory (DFT)

In 1925, Erwin Schrödinger proposed the linear partial differential equation used to study quantum mechanics. The most general form of the Schrödinger equation is defined as:

$$\hat{H}\Psi = E\Psi \tag{1}$$

where $\hat{H}$ is the Hamiltonian operator, and Ψ is the wave function, which is a function of the positions dependent on all electrons, and E is the total energy of electrons in the system. $\hat{H}$ composed of the kinetic (T) energy and the potential (V) of all particles defined as:

$$\hat{H} = T + V \tag{2}$$

$$\hat{H} = -\sum_{i=1}^{n}\frac{1}{2m_e}\Delta r_i - \sum_{I=1}^{N}\frac{1}{2M_I}\Delta R_I + \frac{1}{2}\sum_{i,j}\frac{1}{|r_i - r_j|} + \sum_{I,J}\frac{Z_I Z_J}{|R_i - R_J|} - \sum_{i,I}\frac{Z_I}{|r_i - R_I|} \tag{3}$$

จุฬาลงกรณ์มหาวิทยาลัย
CHULALONGKORN UNIVERSITY

Here, m_e and M_I term refer to mass of electrons and nucleus, r and R denote electron and nucleus coordinate, and Z is a charge. However, this equation is suitable for a small system. Several approximations are proposed to resolve the molecule, having many electrons. Firstly, Max Born and J. Robert Oppenheimer proposed the approximation to reduce the complexity, the so-called Born-Oppenheimer approximation (BOA). This approach is based on the assumption that the ions are much heavier than the electrons (approximately 1840 times), resulting in the kinetic energy of the ions is much smaller than that of the electrons. Furthermore, the motion of an electron is only considered while nuclear coordinates are fixed. Thus, the Schrödinger equation under BOA can be defined as:

$$H = -\sum_{i=1}^{n} \frac{1}{2m_e} \Delta r_i + \frac{1}{2} \sum_{i,j} \frac{1}{|r_i - r_j|} - \sum_{i,I} \frac{Z_I}{|r_i - R_I|} \tag{4}$$

However, this approximation would not be appropriate for complex systems. In 1964, the electronic density proved useful as a variable in the many-body problems by Walter Kohn and Pierre Hohenberg.

2.1.1 Kohn-Sham equation

This approach, which is much simpler than the wave function, includes two fundamental theorems. The first theorem, the ground state properties uniquely depend on the electron density (ρ), and the second, the density can be obtained when an energy functional is minimized. Therefore, it is necessary to find solutions for the energy functional. Subsequently, the Kohn-Sham method was proposed to find self-consistent solutions for the density.

$$V_{KS}[n] = V_{ext}[n] + V_{Hartree}[n] + V_{XC}[n] \tag{5}$$

As a consequence of Equation (5), V_{KS} is Kohn–Sham potential, V_{ext} is the external field, $V_{Hartree}[n]$ is Hartree potential and V_{XC} is the exchange-correlation potential.

จุฬาลงกรณ์มหาวิทยาลัย
CHULALONGKORN UNIVERSITY

$$V_{XC}[n] = \frac{\delta E_{XC}[n]}{\delta n(r)} \tag{6}$$

The density can be calculated by:

$$n(r) = \sum_{i=1}^{N} |\Psi_i(r)|^2 \tag{7}$$

The Kohn–Sham equations is as shown below:

$$\left(-\frac{h^2}{2m}\nabla^2 + V_{KS}(r)\right)\Psi_i(r) = \varepsilon_i\Psi_i(r) \tag{8}$$

Where ε_i is the orbital energy of the corresponding Kohn–Sham orbital $\Psi_i(r)$.

2.1.2 Exchange correlation approximation

Although the exchange-correlation energy (E_{XC}) term is still unknown, many different approximations exist, especially the local-density approximations (LDA) and the generalized gradient approximation (GGA).

Local-density approximations (LDA) is the simple approximation to estimate the density of electrons. The uniform electron density is the primary assumption at all locations. Thus, this approximation is suitable for homogenous gas. Thus, this approximation is still corrected to represent the actual system.

$$E_{XC}^{LDA}[\rho(r)] = \int \rho(r)\, \varepsilon_{XC}^{hom}[\rho(r)]dr \tag{9}$$

For Generalized gradient approximation (GGA), the gradient of electronic density is considered to compensate for many LDA errors, leading to a reasonable description for nonmetallic systems like molecules or oxide surfaces.

จุฬาลงกรณ์มหาวิทยาลัย
Chulalongkorn University

$$E_{XC}^{GGA}[\rho(r), s] = \int E_{XC}^{LDA}[\rho(r)]\rho(r)\, F(s)dr \tag{10}$$

where the F(s) and the s factor can be calculated by:

$$F(s) = (1 + 1.29s^2 + 14s^4 + 0.2s^6)^{1/15} \tag{11}$$

$$s = C\,\frac{|\rho(r)|}{\rho^{4/3}(r)} \tag{12}$$

2.2.3 Periodic boundary conditions (PBC)

The periodic boundary conditions (PBC) are boundary conditions used to model the infinite system, such as heterogeneous catalysts by repeating the small unit cell. The PBC consist of an infinite number of unit cells. One is the single unit cell on which the simulation takes place, while others are copies of unit cells, namely images representing the surroundings in all directions, as illustrated in Figure 3. For surface science and catalysis study, the model can be considered in two dimensions to describe catalyst behaviors, whereas the perpendicular direction to the surface is neglected.

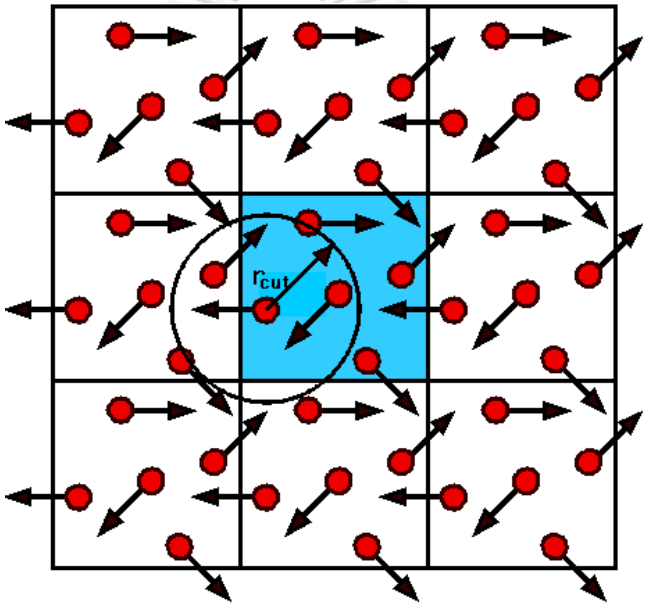

Figure 3 Periodic boundary conditions.

2.2.4 Plane wave based DFT method

The plane wave basis set is the common choice of a basis set used to represent the Kohn-Sham orbitals. These basis sets are suitable for the condensed matter due to the crystalline structure. Moreover, Bloch's theorem was applied to reduce the complexity of the system by introducing the periodic boundary conditions. Based on Bloch's theorem, the Kohn–Sham orbitals for a periodic system can be written as :

$$\Psi_k^{KS}(r) = \sum_G c_{k+G} e^{i(k+G)\cdot r} \tag{13}$$

where k refers to the wave vector, G is the reciprocal lattice vectors, and c_{k+G} is plane wave coefficients. Improving systematic convergence and accuracy is possible by increasing the number of plane waves basis set described by cutoff energy (E_{cut}).

$$E_{cut} = \frac{|k + G_{cut}|^2}{2} \tag{14}$$

Where G_{cut} is the maximum length of the reciprocal lattice vectors.

2.2 Biomass conversion in the aqueous phase

Biomass conversion is a process that produces fuel and a variety of value-added chemicals from local agricultural resources, which can be taken place through multiple transformation routes. Typically, biomass includes bio-oil, sugar, and starch, especially lignocellulose, a promising source non-compete with the edible resource. The major component of lignocellulose, approximately 40-50%, is cellulose, an attractive carbon source for many utilization. For the applications of cellulose, it must be converted into glucose through hydrolysis at the first step. Subsequently, the instantaneous hydrogenation process was performed to produce simple sugar alcohol. Both glucose and sugar alcohol can serve as a precursor for further transformation, for instance, dehydration, oxidation, hydrogenolysis, and reforming. Since the biomass-based intermediate is different from that of petroleum-based. Their large amounts of water and high oxygen contents make them water-soluble. Therefore, these transformation routes mostly proceed in the aqueous phase is shown in Figure 4. The attractive transformation routes can be classified and briefly described as follows.[19,20]

Hydrogenation is one of the critical reactions to saturate bonds in different functional groups, including aldehydes, ketones, furans, carbohydrates, and alkenes. For biomass intermediate, monosaccharides like glucose can be transformed into polyols and light alkanes through consecutive hydrogenation reactions. The conventional catalysts,

including Ni, Ru, Pt on SiO_2, TiO_2, Al_2O_3, and carbon as support materials, have been widely used for the hydrogenation process to achieve this reaction.

Hydrogenolysis consists of two consecutive reactions to selective cleave C-C and C-O bonds by using hydrogen. This reaction is used to produce lower polyols or diol that more profitable. The first step is C-C bonds cleavage for breaking large polyols (xylitol, sorbitol) to lower polyols. The second step is the cleavage of C-O bonds, which is desirable to produce high-value products from polyols, such as the 1,2-propanediol (1,2-PDO) and 1,3-propanediol (1,3-PDO), which are produced from glycerol.

Dehydration is typically used to transform monosaccharides like glucose, fructose, and xylose into furan compounds such as 5-hydroxymethylfurfural (HMF) or furfural. These compound can subsequently be converted into diesel fuel additives, liquid alkane (C_7-C_{15}), polymer and polyurethane foams through various transformation routes.

Aqueous-phase reforming(APR) is an attractive approach for hydrogen production from polyols, sugars, and sugar alcohols due to low energy consumption and high hydrogen production. The product of H_2 can be employed for various applications, e.g., fuel cell, and hydrogenation or hydrogenolysis as a substance. The direct pathway of reaction involves the cleavage of C-C, C-H and O-H bond and consecutively yields CO_2 and H_2 via the water-gas shift (WGS) reaction. For APR, the common catalyst for this reaction is platinum supported on Al_2O_3 based catalyst due to high activity and selectivity towards hydrogen.

จุฬาลงกรณ์มหาวิทยาลัย
CHULALONGKORN UNIVERSITY

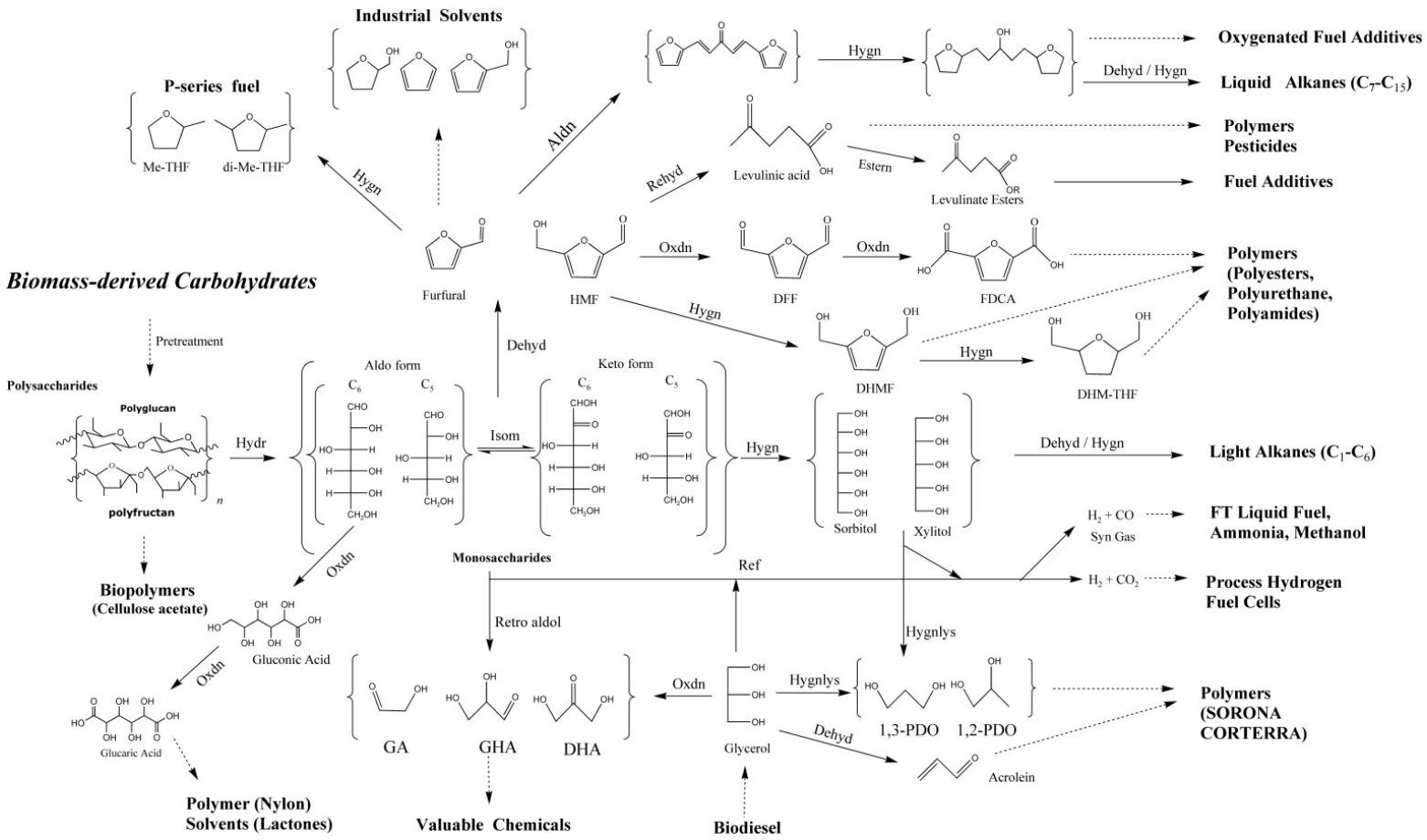

Figure 4 Transformation of carbohydrate-based feedstocks to fuels and chemicals.

2.3 Deactivation on Alumina in the aqueous phase

The possible deactivation taken place in liquid medium is expected that it is similar to deactivation in gas phase, which can be classified into six types: i) fouling, ii) mechanical alterations, iii) metal sintering, iv) poisoning, v) inactive phase formation, and vi) leaching as described in Table 1[11].

Table 1 The general types of deactivation in liquid media. [11]

Type	Mechanism	Description
Mechanical alterations	Loss of active phase or pressure build-up	Crushing or attrition between catalyst particles
Metal sintering	Decrease in the exposed active sites	Loss of surface area by increasing crystal size
Leaching	Loss of active sites	Active phase dissolution/release into the liquid medium
Fouling	Lack of accessibility	Physical deposition with chemical species on the surface (fouling/coking)
Poisoning	Decline of intrinsic activity	Chemisorption of species that could be detrimental to active sites
Formation of new inactive phases	New phases are not active	Reactions affecting the catalyst components leading to different phases

จุฬาลงกรณ์มหาวิทยาลัย
Chulalongkorn University

The alteration in liquid media mainly involves attrition and crushing, resulting in size reduction and particle cracking, making it suitable for investigation on a large scale than an atomic scale. Also, the sintering and leaching are mainly associated with the metal rather than support. Hence, three types of deactivation cause, including mechanical alterations, sintering, and leaching, are not considered in this work.

2.4 Coking

Coking is one of the deactivation caused by unavoidable carbonaceous deposition on the catalyst surface, leading to blockage of active sites or pores and then activity loss. The reactions for which coke deposition mainly contribute include oxidative dehydrogenation, isomerization, hydrogenation, and reforming. Due to the complexity of the coke feature, it can be explained in terms of (i) content, (ii) position and morphology, and (iii) formation mechanism as depicted below in Figure 5. [21]

I. **Content:** The factor influences coke content, including the operating conditions, space time, and the aromatic structure in the feed, promotes coke deposition since the polymerization of aromatics precursor.

II. **Position and morphology**: The formed coke can be divided into three types based on their morphology: encapsulating, filamentous, and pyrolytic coke; these cokes take place on metal, metal-support interface, and support, respectively.

III. **Formation mechanism**: The encapsulating coke originate from the feed adsorption on metal sites and further condensation/polymerization of coke until full covering metal sites. For filamentous coke, the precursors are adsorbed on metal sites. After that, it dissociates into atomic carbon and then diffuses through metal. It is deposited in the metal-support interface, and these metal sites are removed from the surface eventually. The last, pyrolytic coke is produced by precursor cracking, particularly acid supports like γ-Al_2O_3, which tends to yield a higher coke content since it favors cracking reactions.

CHULALONGKORN UNIVERSITY

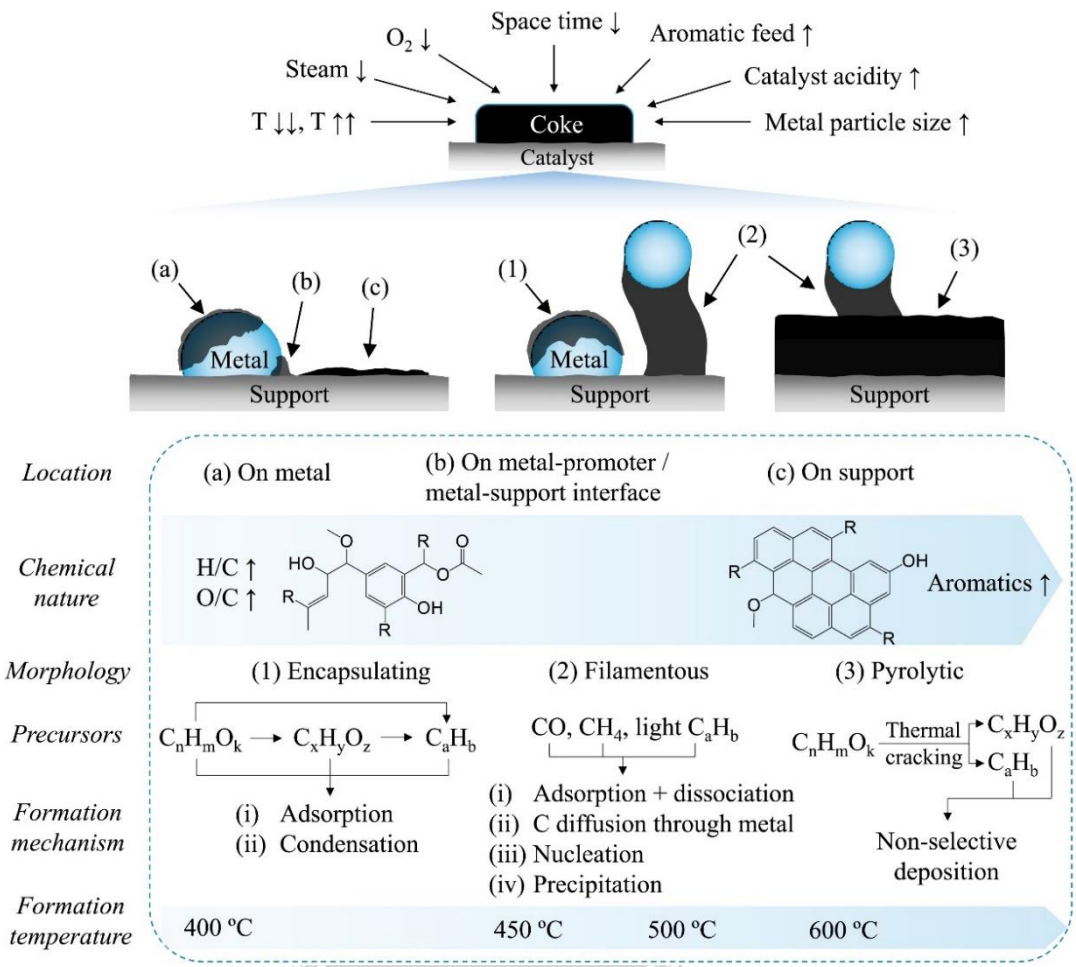

Figure 5 The characteristic of coke deposited on catalyst in reforming reactions. [21]

จุฬาลงกรณ์มหาวิทยาลัย
Chulalongkorn University

Moreover, Argyle, M. and C. Bartholomew[15] summarized the coke formation on metal oxide and sulfide catalysts that involve cracking reactions with coke precursors. Their mechanism mainly consists of three parts: polymerization of alkenes, alkenes cyclization, and polyaromatic formation, as illustrated in Figure 6. Hence, the two types of cokes are emphasized in this study, including initial coke like atomic carbon and cyclic coke stand for polynuclear aromatic structure.

(a) Polymerization of alkenes

Step 1 : Reaction of olefin with Bronsted acid from secondary carbenium ion:

$$H_2C{=}CHCH_3 + HX \rightleftharpoons CH_3{-}\underset{+}{C}HCH_3 + X^- \quad (1)$$

Step 2 : Condensation reaction of C_3 carbocation with a C_3 olefin to form a condensed, branched C_6 product with a carbenium ion:

$$CH_3{-}\underset{+}{C}HCH_3 + H_2C{=}CHCH_3 \rightleftharpoons CH_3{-}CHCH_3{-}CH_2{-}\underset{+}{C}HCH_3 \quad (2)$$

Step 3 : Reaction of carbenium ion with Bronsted base to form olefin:

$$CH_3{-}\overset{CH_3}{CH}{-}CH_2{-}\underset{+}{C}H{-}CH_3 + X^- \rightleftharpoons CH_3{-}\overset{CH_3}{CH}{-}CH_2{-}CH{-}CH_2 + HX \quad (3)$$

(b) Cyclization from olefin

Step 1 : Formation of an allylic carbocation by reaction of a diene with a primary carbocation:

$$R_1^+ + R_2{-}CH{=}CH{-}CH{=}CH{-}CH{-}CH_2CH_3 \rightleftharpoons R_1H + (R_2{-}CH{\cdots}CH{\cdots}CH{\cdots}CH{\cdots}CH{-}CH_2CH_3)^+ \quad (4)$$

Step 2 : Reaction of an allylic carbocation with Bronsted base to form triene:

$$X^- + (R_2{-}CH{\cdots}CH{\cdots}CH{\cdots}CH{\cdots}CH{-}CH_2CH_3)^+ \rightleftharpoons R_2{-}CH{=}CH{-}CH{=}CH{-}CH{=}CHCH_3 + HX \quad (5)$$

Step 3 : Cyclization of a triene to form a substituted cyclohexadiene

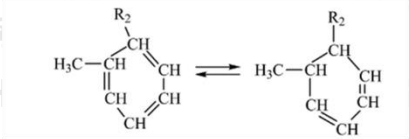

(6)

Step 4 : Formation of a tertiary carbocation:

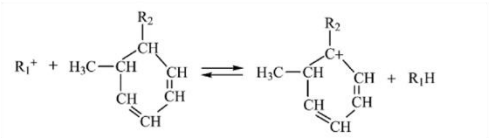

(7)

Step 5 : Reaction of a tertiary carbocation with Bronsted base to form a substituted benzene:

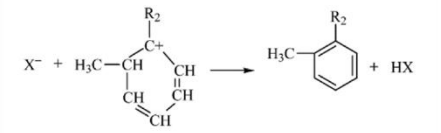

(8)

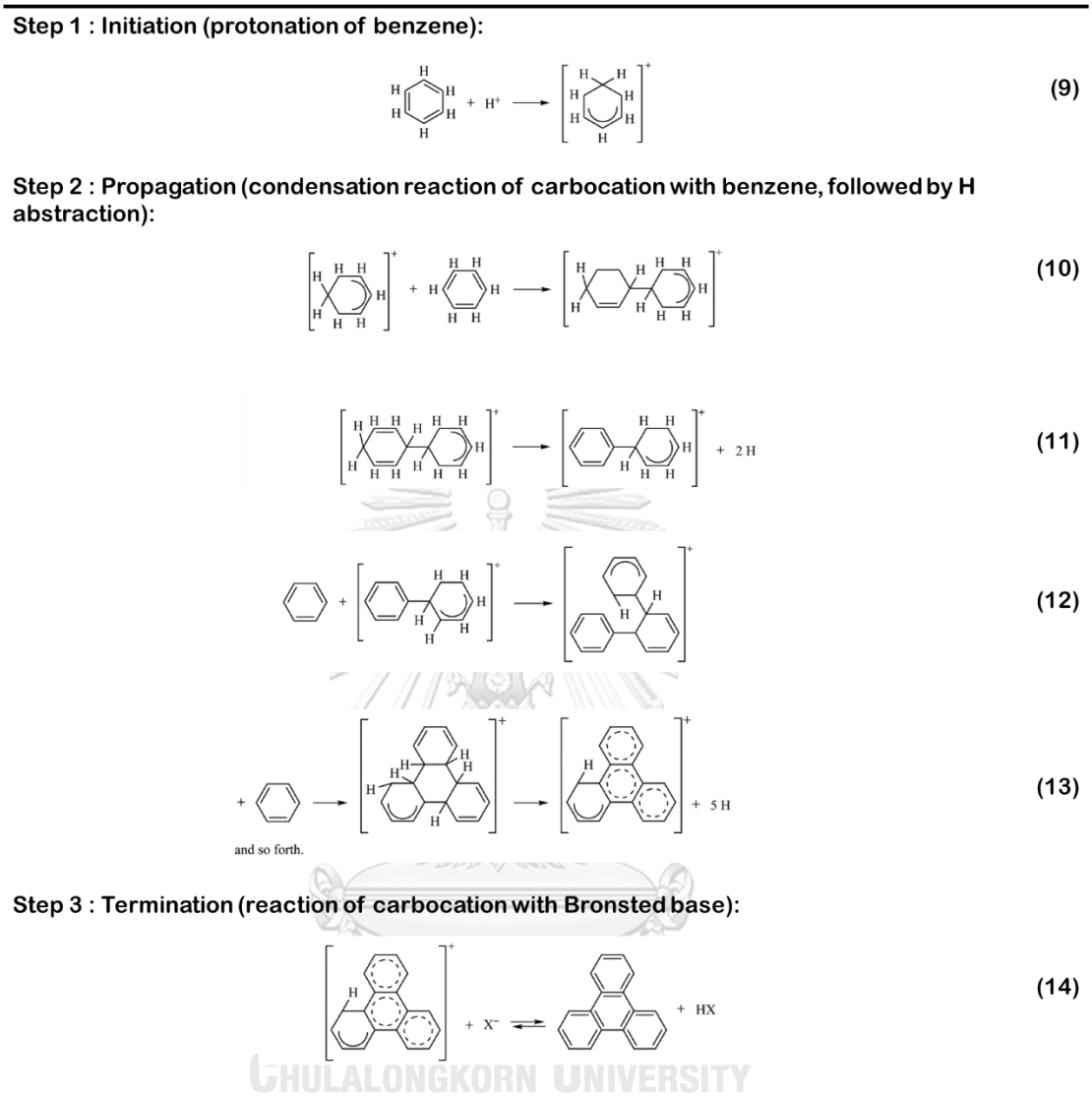

Figure 6 The coke formation mechanism on metal oxide and sulfide catalysts consisting of three parts: (a) polymerization, (b) cyclization, and (c) polyaromatics formation.[15]

2.5 Phase transformation

In the aqueous phase reaction, the growth of the inactive phase, especially boehmite, is thermodynamically driven under hydrothermal conditions. The first step leading to transformation is hydration, and the reactive sites for hydrated γ-Al_2O_3 were demonstrated in the theoretical study via ab initio molecular dynamics[22]. This irreversible transformation detrimentally affects to collapse of the active structure, loss of surface area, and change of its intrinsic properties, such as acidity. Besides, this

transformation results in the sintering of the metal particles. These reasons are leading to the challenge to prevent the transformation of γ-Al_2O_3 in the aqueous phase:

I. The addition of metal, such as nickel and platinum, can retard the phase transformation compared to the bare γ-Al_2O_3 by hindering specific sites on the surface responsible for initial hydration.

II. Doping of additives, such as carbon, SiO_2, and polyol molecules could enhance the water-resistance and impede the hydration of γ-Al_2O_3, which initiation step leading to transformation.

2.6 Oxygen vacancy

Oxygen vacancy is one type of deficient. In the metal oxide catalysts, the oxygen vacancy can be produced during reactions such as oxidation by taking oxygen atom from the surface. Moreover, water-gas shift reaction (WGSR) and oxidative dehydrogenation can easily exchange oxygen, especially reducible metal oxides groups such as TiO_2, WO_3, and CeO_2[16]. When oxygen is removed, the electrons on the material were trapped, generating a new state in the bandgap between the valence band (VB) and the conduction band (CB). The capacity in electron trapping depends on the orbital difference of oxygen and metal in metal oxide material. On the other hand, the nonreducible metal oxide group, consisting of SiO_2, MgO, and Al_2O_3, required costly energy to form vacancy. Due to a very large bandgap (typically >3 eV), the cation empty states available on CB is too high to migrate the excess electron from the oxygen 2p orbital states in VB. Even though γ-Al_2O_3 is a nonreducible metal oxide group, oxygen vacancy can be induced by increasing reducibility, either by varying preparation or metal doping. As aforementioned, oxygen vacancies play a role in change catalytic reactivity[23] and reaction pathways[24,25] and tailor the essential properties[26] of metal oxide. Therefore, it may influence the deactivation of γ-Al_2O_3.

2.7 Literature reviews

Lei, N., *et al.* investigated the deactivation on Pt/WO_3/γ-Al_2O_3 catalyst during the hydrogenolysis reaction of glycerol for 700 h. The result shows that decreasing Pt-WO_x interfacial sites raised from the agglomeration of platinum nanoparticles on the surface is a significant cause of catalyst deactivation. Moreover, the weight loss occurred during Thermogravimetric analysis (TGA) and Temperature Programmed Oxidation

(TPO) analysis. The first, 1.5 % weight loss, was detected below 150 °C due to water evaporation. The second, 3.6 % weight loss appeared at 200–500 °C and described coke on the surface. The coking may cause to deactivation of the γ-Al_2O_3 based catalyst.[13]

Matsushita, K., *et al.* studied initial coke formation and its modified properties on Mo/γ-Al_2O_3 catalyst during hydrotreating of Kuwaiti atmospheric residue. The results show that the formed cokes are divided into soft coke (S) and refractory coke (R). The S/R ratio shifted towards more refractory coke, which is strongly adsorbed at the catalyst support. Moreover, the used catalyst of 1, 12, 48, and 120 h times on stream period was examined with the tetrahydrofuran (THF) extraction. The result demonstrated the aliphatic and aromatic cokes on the catalyst surface, and the coke became more aromatic structure with increasing the times on steam.[12]

Y. Dang studied the adsorption behavior of polycyclic aromatic hydrocarbons, including naphthalene, anthracene, and phenanthrene on γ-Al_2O_3 (110) surfaces with different hydroxyl concentrations, 5.9 and 8.9 OH/nm^2, by DFT method with GGA. The adsorption energy increase with the size of the aromatic molecule in order: anthracene > phenanthrene > naphthalene. While considering the geometry effect, the linear aromatic is stronger adsorbed than the non-linear aromatic with the same aromatic ring due to the higher electron density.[27]

Rinaldi, R., *et al.* investigated the deactivation of γ-Al_2O_3 in epoxidation using aqueous 70% H_2O_2 for 24 h. The result demonstrated that water cause chemical and physical changes of γ-Al_2O_3 due to transformation into a less active phase, including boehmite and an amorphous aluminum trihydroxide. This phase transformation mainly contributes to catalyst deactivation. The adsorbed organic molecules also have a detrimental effect on the active site for epoxidation on γ-Al_2O_3.[9]

Ravenelle, R. M., *et al.* studied the structural change of γ-Al_2O_3 based catalyst under aqueous phase reforming conditions for ten h. The various techniques were applied to identify the change of catalyst during water treatment. The X-Ray Diffraction (XRD) results demonstrated that γ-Al_2O_3 is converted into a boehmite phase with a significant surface area decrease. Additionally, the pyridine adsorption and IR spectroscopy were used to determine the acidity of the catalyst. It was found that acidity decreased with increasing phase transformation. Besides, when considering Ni/γ-Al_2O_3 and Pt/ γ-

Al_2O_3, the presence of metal particles retard phase change into boehmite compared to bare γ-Al_2O_3.[10]

Yazdanmehr, M., *et al.* investigated a real γ-Al_2O_3 containing defect site in structure, oxygen, or aluminium vacancies based on DFT calculations. The defect can produce the interstate bands between the valence band and conduction band, which agrees with the experimental result. This result shows that the formation of Al vacancy generates acceptor-like interstate bands, those of oxygen conversely, vacancy generates donor-like interstate bands below the conduction band.[17]

X. Krokidis [28] examined the structural transformation of γ-AlOOH into γ-Al_2O_3 by molecular dynamics (MD) simulations. This transformation consists of two main steps: the collapse of the boehmite structure and aluminium migration. The equilibrium structure derived from this dehydration process is composed of 25-31% tetrahedral aluminium, corresponding with nuclear magnetic resonance (NMR) results. Also, the simulated X-ray diffraction (XRD) patterns confirmed reliable of model structure γ-Al_2O_3.

Y. Noel[29] summarized the various space groups of boehmite to identify the most stable structure. The space groups were considered $Cmc2_1$, $P2_1/b$, and $P2_1ab$, which these space groups differ for the hydrogen atoms orientation as depicted in Figure 7, whereas the Al-O configuration remains similar to the Cmcm space group. The previous study[30] confirmed that these space groups are more stable than Cmcm. Also, $Cmc2_1$ is the most symmetric least-energy structure compared to other space groups. Moreover, Digne *et al.*[31] studied the surface energies and interfacial energies in water of γ-AlOOH, including (010),(100), (001), and (101) planes by using ab initio molecular dynamics. The result demonstrated that (010) facet is the main surface plane and exhibits the lowest surface energy in vacuum at 0 K and in water at T= 350 K.

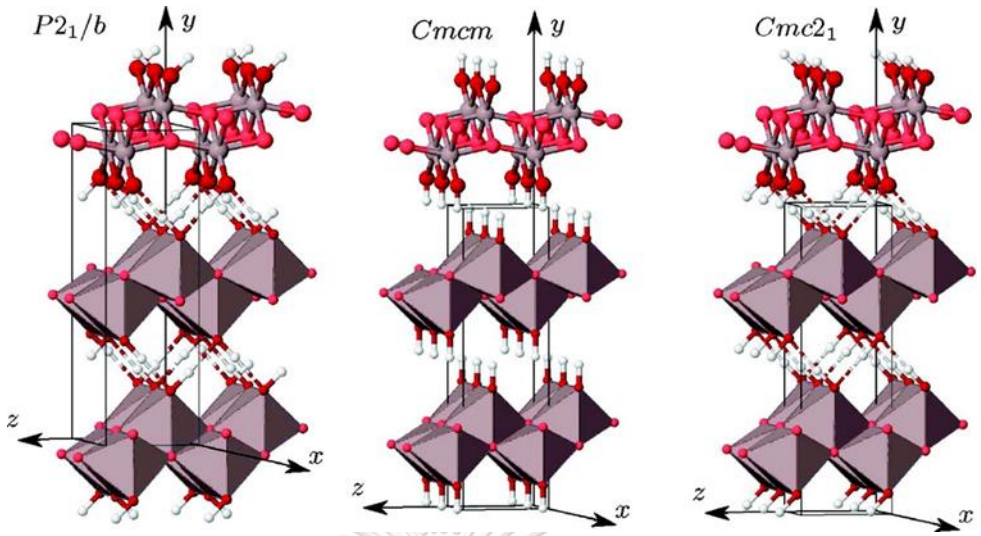

Figure 7 The space group of boehmite: P21/b (left), Cmcm (center), and Cmc21 (right).[29]

จุฬาลงกรณ์มหาวิทยาลัย
CHULALONGKORN UNIVERSITY

CHAPTER 3
COMPUTATIONAL DETAILS AND METHODOLOGY

3.1 Computational methods and parameter

All DFT[32] calculations were systematically performed using Vienna ab initio simulation package (VASP)[33,34] program with the projector augmented wave (PAW) potential[35,36]. The generalized gradient approximation (GGA) corresponding to exchange-correlation functionals by Perdew, Burke, and Ernzerhof (PBE)[37] is employed. Moreover, the Van der Waals correction of DFT-D3 dispersion proposed by Grimme *et al*.[38] was also included. During optimization, the kinetic energy cutoff was set as 450 eV, and the Monkhorst-Pack Grids grid, which is used to construct the Brillouin-zone[39], was set as 5x3x1. Furthermore, the structural optimization was performed using the conjugate gradient method[40] with the energy convergence criteria of 1×10^{-6} eV and atomic force convergence criteria of 0.01 eV/Å. Besides, the Gaussian smearing with smearing width of 0.05 eV was utilized to determine the partial occupancies of each orbital[41].

The interaction between interaction between cokes and surface was described via the adsorption energy (E_{ads}) which is calculated as:

$$E_{ads} = E_{coke\text{-}surface} - (E_{isolated\text{-}coke} + E_{surface}) \quad (15)$$

Where $E_{coke\text{-}surface}$ refers to the total energy of the adsorption system (adsorbed coke on the surface), $E_{isolated\text{-}coke}$ refers to the total energy of an isolated coke optimized in a vacuum region, and $E_{surface}$ refers to the total energy of the clean surface. A negative E_{ads} value indicates an attractive interaction between coke and surface. Also, the magnitudes refer to the strong/weak interaction between the coke and surface.

To described electron distribution ($\Delta\rho$) on the surfaces after coke adsorption, the Bader charge analysis[42,43] was calculated as follows:

$$\Delta\rho_{coke,\ surface} = \Delta\rho^{ads}_{coke,\ surface} - \Delta\rho^{clean}_{coke,\ surface} \quad (16)$$

The $\Delta\rho^{clean}_{coke,\ surface}$ represents the electron density change of isolated coke and the clean surface before coke adsorption, while the $\Delta\rho^{ads}_{coke,\ surface}$ indicates the electron density change of adsorbed system. All electron density changes were calibrated with valence electrons of Al, O, H, and C atoms.

Also, the charge density difference is usually applied to indicate active site and the interaction between surface and coke as follows:

$$\Delta\rho = \rho_{system}\text{-}(\rho_{clean}+\rho_{coke}) \tag{17}$$

The ρ_{system} refers to the electron density of the adsorption system, whereas the ρ_{coke} and ρ_{clean} represent the partial charge of isolated coke and the clean surface with the fixed positions of the adsorption system.

$$\Delta G_{ads} = E_{ads} + \Delta ZPE - RT \ln Q_{vib} \tag{18}$$

Where E_{ads} is the adsorption energy, R is the gas constant, T is the absolute temperature, The Q_{vib} is the total vibrational partition function, and ΔE_{ZPE} is the zero-point energy that can be calculated by the following equation

$$E_{ZPE} = \sum \frac{h\nu_i}{2} \tag{19}$$

where h is the Planck's constant, and ν_i represent the vibrational frequency.

3.2 Structure Model

3.2.1 The γ-Al_2O_3 surface

The non-spinel structure model proposed by Digne *et al.*[44,45] was chosen to represent the bulk structure of γ-Al_2O_3 in this work. The unit cell contains 40 atoms (16 Al and 24 O). The optimized cell parameters are a = 5.52, b = 8.33, and c = 8.02. The calculations of the total density of states demonstrate that the bandgap of γ-Al_2O_3 is 1.28 eV, in agreement with the previous study [46]. The most encountered termination of

γ-Al_2O_3 is the (110) facet. For the slab model, γ-Al_2O_3 (110) surface consisted of four-layer in the periodic supercells and approximately ~15 Å vacuum region to avoid periodic interaction as depicted in Figure 8.

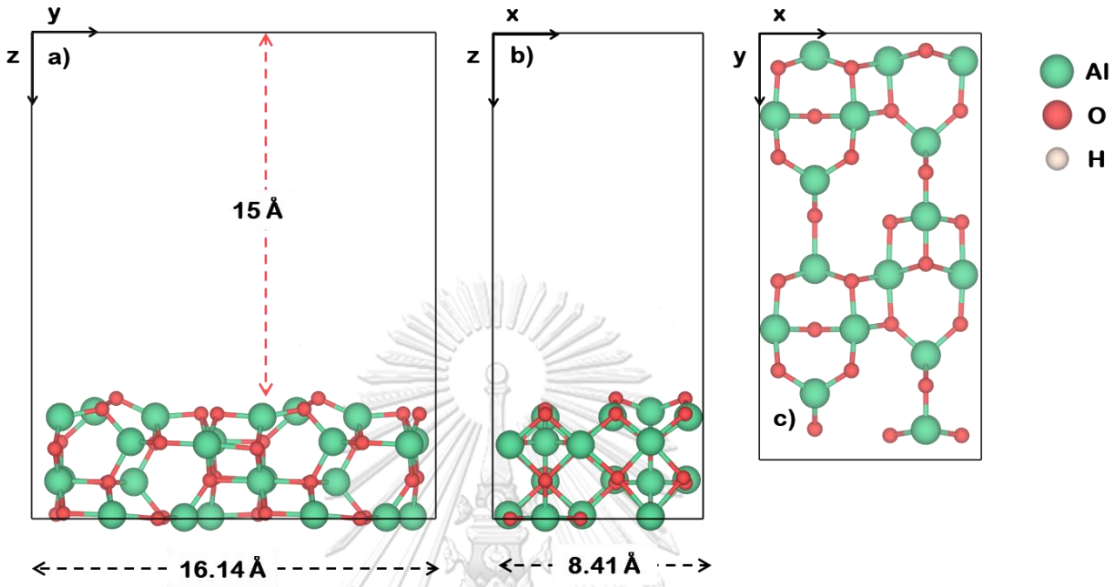

Figure 8 Surface model for γ-Al_2O_3 (110) projected along a) the (010)-direction, b) the (100)-direction, and c) the (001)-direction. The Al and O are indicated by green and red, respectively.

จุฬาลงกรณ์มหาวิทยาลัย
Chulalongkorn University

3.2.2 The OH/ γ-Al_2O_3 surface

The partial hydrated surface was generated to represent the surface during aqueous phase reaction. The OH/γ-Al_2O_3 (110) structure derived from γ-Al_2O_3 surface modeled by Digne *et al*. with two water molecules per unit cell based on previously reported of Wischert, R., *et al*.[47,48] The surface model consists of four atomic layers and ~15 Å vacuum with a dimension of 8.41 Å × 16.14 Å × 19.41 Å. as illustrated in Figure 9. Two top layers were relaxed during surface optimization for both γ-Al_2O_3 (110) and OH/γ-Al_2O_3 (110) surface, and other layers were fixed in the local position from bulk optimization.

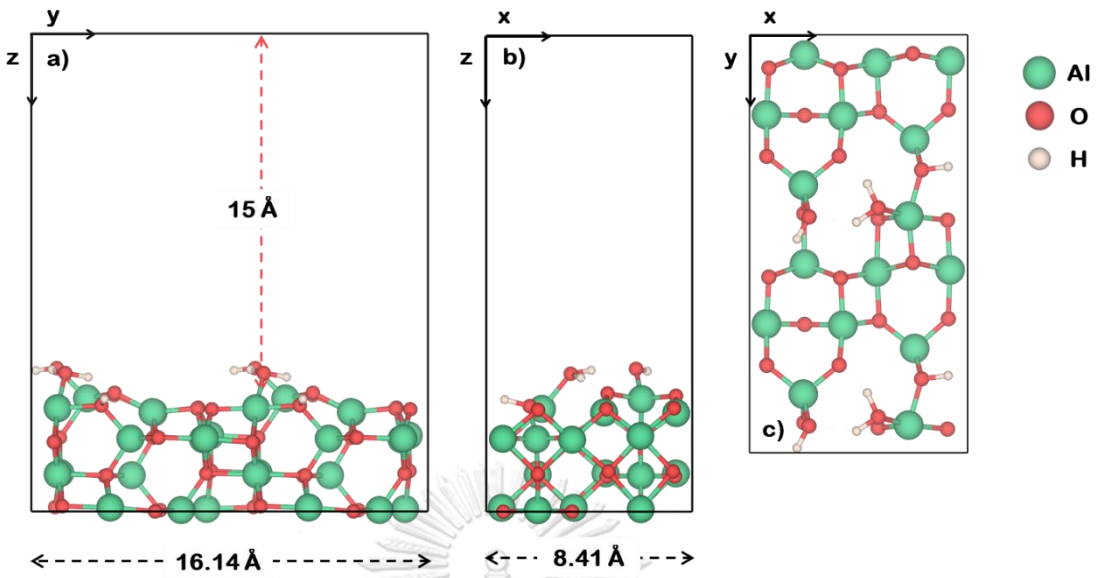

Figure 9 Surface model for OH/γ-Al_2O_3 (110). projected along a) the (010)-direction, b) the (100)-direction, and c) the (001)-direction. The Al, O and H are indicated by green, red, and orange.

3.2.3 The γ-AlOOH surface

Boehmite exhibits a layered structure with orthorhombic symmetry. The $Cmc2_1$ space groups are appropriate for describing boehmite due to the calculated structural parameters in great agreement with the experimental data and the most symmetric least-energy structure[29,30]. The unit cell contains 16 atoms (4 Al, 4 H and 8 O). The optimized cell parameters are a = 2.87, b = 11.91, and c = 3.72. of γ-AlOOH. For the slab model, γ-AlOOH (010), the main termination, was constructed using two-layer in the periodic supercells and consisted of approximately ~15 Å as a vacuum region depicted in Figure 10. During surface optimization, bottom layer and hydrogen-interlayer were fixed in local position, and another layer was relaxed.

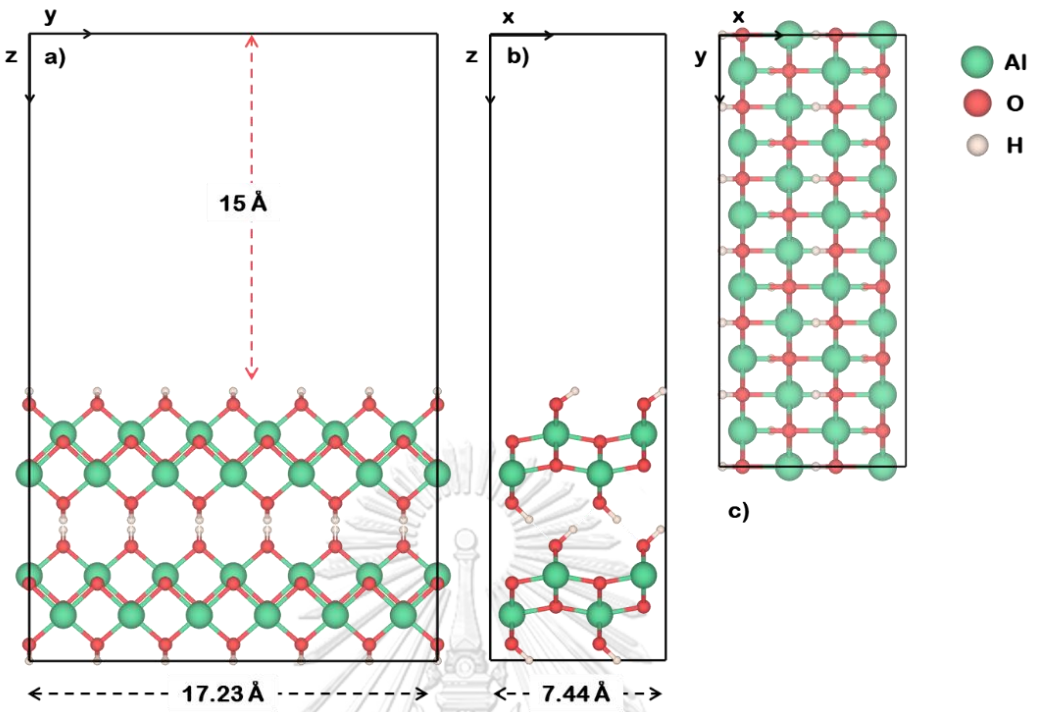

Figure 10 Surface model for γ-AlOOH (010) projected along a) the (010)-direction, b) the (100)-direction, and c) the (001)-direction. The Al, O and H are indicated by green, red, and ivory, respectively.

จุฬาลงกรณ์มหาวิทยาลัย
CHULALONGKORN UNIVERSITY

3.2.4 The isolated-coke molecule

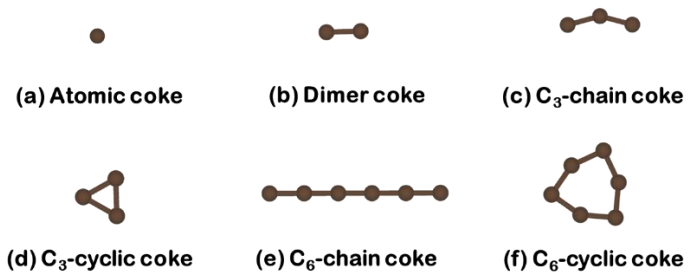

Figure 11 The various types of molecules used in coke adsorption.: (a) C_1-atomic coke, (b) C_2-dimer coke, (c) C_3-chain coke, (d) C_3-cyclic coke, (e) C_6-chain coke and (f) C_6-cyclic coke.

CHAPTER 4
RESULTS AND DISCUSSIONS

4.1 Coke behavior on γ-Al_2O_3

4.1.1 Coke adsorption on γ-Al_2O_3

To understand the interaction between coke and γ-Al_2O_3 (110) surface, the adsorption of various types of coke, including atomic coke (C_1-atomic), diatomic coke (C_2-diatomic), and dimer coke(C_2-dimer), were firstly investigated. The most stable configuration is illustrated in Figure 12, and the E_{ads} are summarized in Table 2. For the initial stage of coke formation, both C_1-atomic and C_2-dimer prefer to adsorb on the oxygen site by connecting to O(1) atom of γ-Al_2O_3 (110) surface with the E_{ads} of -3.86 eV and -5.89 eV, respectively. For the C_2-diatomic system, two atoms of C_1 can be adsorbed on two oxygen sites of γ-Al_2O_3 (110) surface with E_{ads} of -7.63 eV. The first C_1 atom labeled as C(1) is adsorbed on the O(1) site, which is similar to C_1-atomic adsorption, while the other labeled as C(2) is adsorbed to the O(2) site. Indeed, the O(1) and O(2) are similar, but they are located in different periodic images. It implies that if the most favorable site O(1) on the γ-Al_2O_3 (110) surface is still uncovered, the second C_1-atomic will be further adsorbed. Moreover, the double E_{ads} value of C_2-diatomic compares to the C_1-atomic system signifying that the C_2-diatomic behave like C_1-atomic individually adsorbed on the surface. In other words, there is only interaction between C(1) or C(2) and γ-Al_2O_3(110) surface. Interestingly, the second atom of coke cannot separately adsorb around the first adsorbed C(1) on γ-Al_2O_3 (110) surface observed by the transformation of C_2-diatomic to C_2-dimer with the E_{ads} is -4.74 eV after the optimization process. Therefore, the increase in the number of atomic coke adsorbed on the surface or the diffusion of atomic coke proceed to coke dimerization, eventually leading to coke evolution.

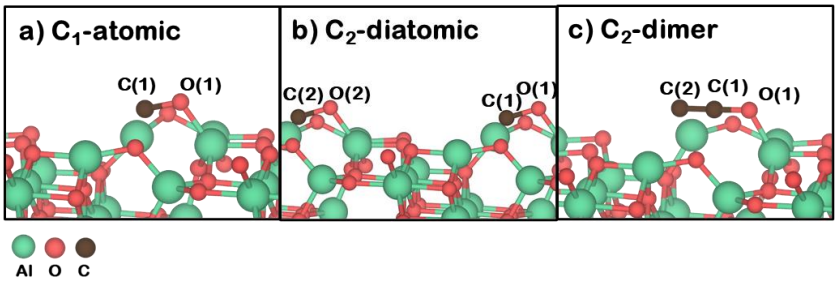

Figure 12 The most stable configuration of coke on γ-Al_2O_3 (110) surface in the initial stage , including a) atomic coke, b) diatomic coke, and c) dimer coke. The Al, O, and C are indicated by green, red, and brown.

Table 2 Adsorption energy and bond distance of coke adsorption on γ-Al_2O_3 (110) surface.

Molecule	Coke form	E_{ads}(eV)	Bond distance (Å)	
			C(1)-O(1)	C-C $^{(avg)}$
C_1	atomic	-3.86	1.29	-
C_2	diatomic	-7.63	1.42	1.37
C_2	dimer	-5.89	1.28	1.26
C_3	chain	-3.23	1.30	1.34
C_3	cyclic	-4.81	1.30	1.40
C_6	chain	-4.04	1.34	1.29
C_6	cyclic	-4.50	1.40	1.38

After the coke dimerization, the formation of higher coke (three and six atoms of carbon) was also investigated to describe coke evolution on γ-Al_2O_3(110) surface that the most geometry of each coke is shown in Figure 13, and The E_{ads} of each coke is reported in Table 2. In this study, the occurrence of coke evolution can be taken place into two forms: one is aliphatic coke or chain structure, and another is cyclic coke. The aliphatic form of three and six atomic coke can be represented as C_3-chain and C_6-chain, respectively. Moreover, the cyclic form of three and six atomic coke can be defined as C_3-cyclic and C_6-cyclic, respectively. The E_{ads} of C_3-chain, C_6-chain, C_3-cyclic, and C_6-

cyclic are -3.23 eV, -4.04 eV, -4.81 eV, and -4.50 eV, respectively. The more negative value of cyclic coke implies that the formation of cyclic coke during coke evolution is more energetically favorable than that of the aliphatic coke, in good agreement with previous experimental investigation[12]. However, the coke-surface interaction of all higher cokes, including aliphatic and cyclic cokes on γ-Al_2O_3(110) surface are still weaker than that of C_2-dimer due to a steric effect which appears on a high coke species demotes interaction between a carbon atom of coke and active species of γ-Al_2O_3(110) surface.

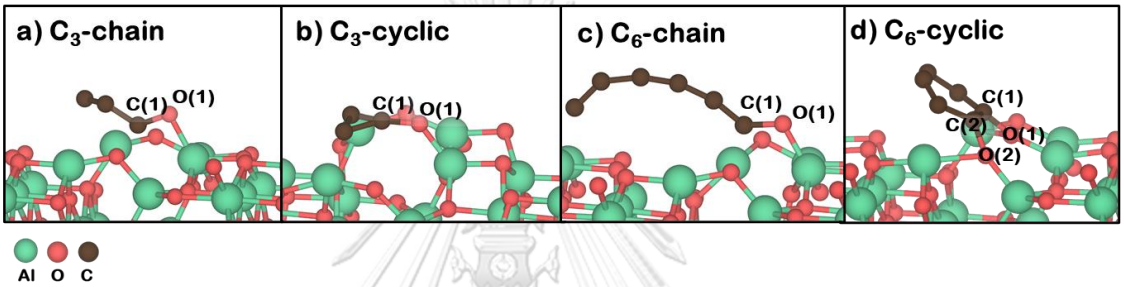

Figure 13 The most stable configuration of coke adsorption on the γ-Al_2O_3 surface in the polymerization stage, including a) C_3-chain, b) C_6-chain, c) C_3-cyclic, and d) C_6-cyclic. The Al, O, and C are indicated by green, red, and brown.

4.1.2 Coke evolution on γ-Al_2O_3

The mechanism of coke evolution initiating from the smallest coke deposition to higher coke formation was investigated. Moreover, the proposed mechanism of coke agglomeration was considered through the continuous growth based on Langmuir–Hinshelwood (LH) pathway, as displayed in Figure 14. The C_1-atomic adsorption was proposed as a beginning step. Then, the C_1-atomic can be enlarged to C_2-dimer by forming with the nearest C_1-atomic. After that, the C_2-dimer can be polymerized as two isomers of higher coke of C_3: one is a long-chained C_3 defined as C_3-chain, and another is a cyclic form of C_3 defined as C_3-cyclic. Investigation of higher coke evolution is proceeded to C_6, referring to the first unit of graphitic coke, which is the crucial cause for catalyst deactivation. Moreover, the aliphatic form of C_6 coke or C_6-chain is also systematically investigated comparing to C_6-cyclic.

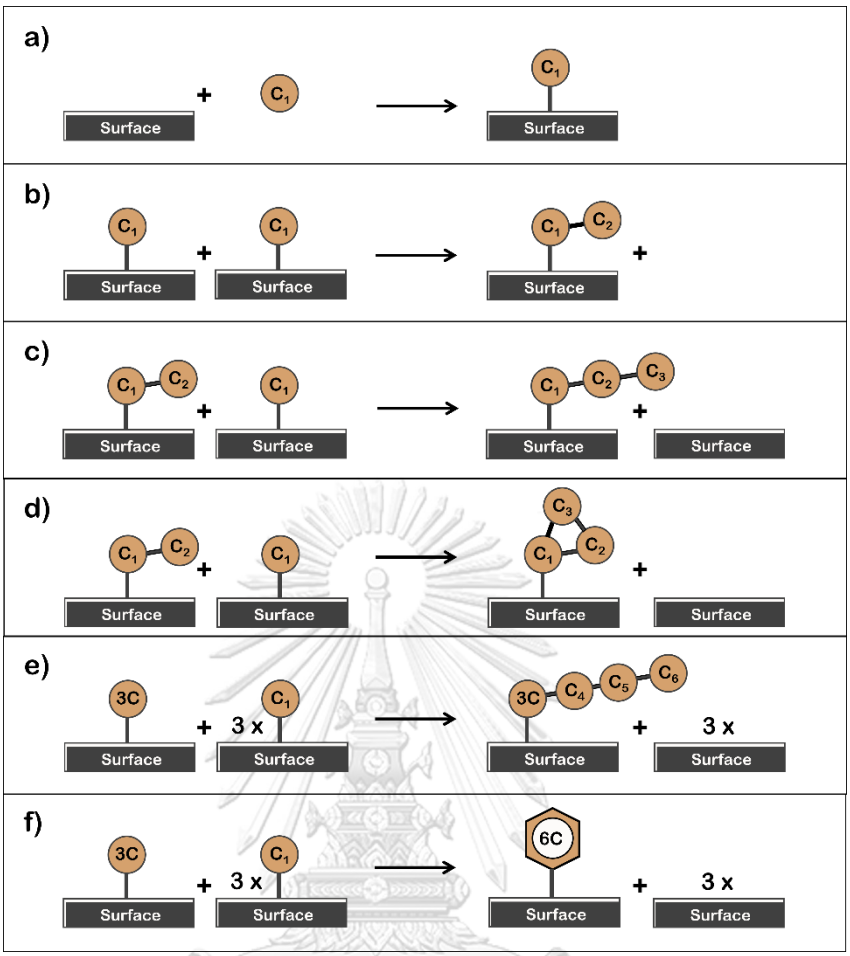

Figure 14 Proposed mechanism of coke evolution through the continuous growth on catalyst surface based on Langmuir–Hinshelwood (LH) mechanism.

The energy required for the continuous growth from initial coke (C_1) into higher coke (C_6) was described via the relative formation energy, which is calculated as:

$$E_{form} = E_{product} - E_{reactant} \tag{20}$$

(a) $E_{form,C_1} = \left(E_{C_1/surface}\right) - \left(E_{clean\ surface} + E_{isolated\ C_1}\right)$

(b) $E_{form,C_2\text{-dimer}} = \left(E_{C_2\text{-dimer/surface}} + E_{clean\ surface}\right) - \left(2 \times E_{C_1/surface}\right)$

(c) $E_{form,C_3\text{-chain}} = \left(E_{C_3\text{-chain/surface}} + E_{clean\ surface}\right) - \left(E_{C_2\text{-dimer/surface}} + E_{C_1/surface}\right)$

(d) $E_{form,C_3\text{-cyclic}} = \left(E_{C_3\text{-chain/surface}} + E_{clean\ surface}\right) - \left(E_{C_2\text{-dimer/surface}} + E_{C_1/surface}\right)$

(e) $$E_{form,C_6\text{-chain}} = \left[E_{C_6\text{-chain/surface}} + (3\times E_{\text{Clean surface}})\right] - \left[E_{C_3\text{-chain/surface}} + \left(3\times E_{C_1\text{/surface}}\right)\right]$$

(f) $$E_{form,C_6\text{-cyclic}} = \left[E_{C_6\text{-chain/surface}} + (3\times E_{\text{Clean surface}})\right] - \left[E_{C_3\text{-chain/surface}} + \left(3\times E_{C_1\text{/surface}}\right)\right]$$

The $E_{coke/surface}$ refers to the total energy of the adsorption system (adsorbed coke on the surface), while $E_{isolated\ C_1}$ and $E_{Clean\ surface}$ refer to the total energy of an isolated coke in a vacuum, and the total energy of the clean surface, respectively. The negative value of the formation energy indicated that the elementary step would proceed forward converting reactants into products, and the magnitude of them refer to the preferable form of the product. The relative formation energy of coke on the γ-Al_2O_3 surface is reported in Table 3.

The relative ΔE_{form} diagram of coke evolution from coke initiation (C_1-atomic) to C_6 formation (aliphatic and cyclic forms) on γ-Al_2O_3(110) surface is illustrated in Figure 15. After the C_1-atomic adsorption in the initial step, the dimerization forming C_2-dimer can take place with ΔE_{form} of -5.16 eV. Then, the C_2-dimer can be agglomerated to C_3, classified into two possible forms of C_3-chain (ΔE_{form} = -1.69 eV) and C_3-cyclic (ΔE_{form} = -2.76 eV). After that, the C_3 coke is continuously enlarged to C_6 forms of C_6-chain and C_6-cyclic with the ΔE_{form} of -9.51 eV and -10.30, respectively. Decrement of the relative ΔE_{form} during coke evolution is the function of C atom loading referring to the size of enlarged coke directly. The more negative value of the relative ΔE_{form} during higher coke formation indicates that the occurrence of coke agglomeration on γ-Al_2O_3(110) surface is thermodynamically favorable.

In addition, the formation of C_3-cyclic after coke dimerization and C6-cyclic in the final state of this investigation reveals that the formation of a cyclic structure is more energetically stable than chain structure. Especially, the C_6-cyclic refers to a basic unit of the graphitic coke towards the catalyst deactivation; hence the consideration of a higher coke after C_2-dimer will focus only on the C_6-cyclic form for further discussion.

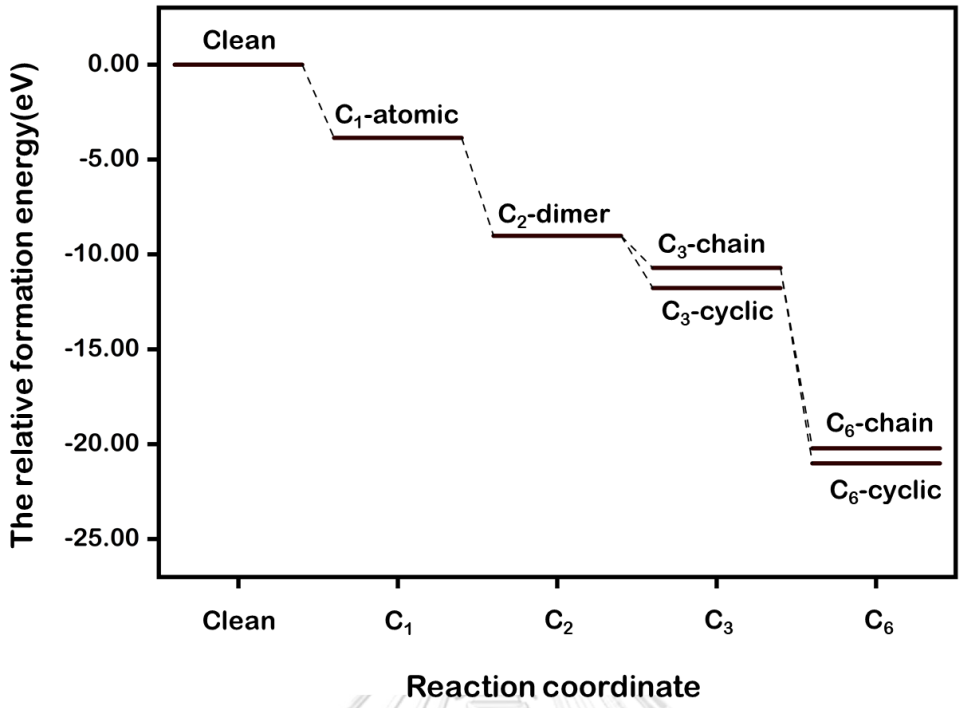

Figure 15 The relative ΔE_{form} diagram for the coke evolution on γ-Al_2O_3 (110) surface based on LH mechanism.

Table 3 The formation energy of coke on γ-Al_2O_3 (110) surface.

Step	Reaction pathway	The ΔE_{form} (eV)	The relative ΔE_{form} (eV)
(a)	C_1 atomic adsorbed on clean surface	-3.86	-3.86
(b)	C_1 atomic to C_2 dimer coke	-5.16	-9.02
(c)	C_2 dimer to C_3 chain coke	-1.69	-10.71
(d)	C_2 dimer to C_3 cyclic form	-2.76	-11.78
(e)	C_3 chain to C_6 chain coke	-9.51	-20.22
(f)	C_3 chain to C_6 cyclic form	-10.30	-21.01

4.1.3 Feasibility of coke evolution

According to the previous section, the dimerization reaction, transforming the diatomic into dimer form, could be a beginning point of the continuous growth of coke on all surfaces. Therefore, dimerization has gained attention as the simplest path for explaining the feasibility of coke evolution. The feasibility of any chemical reaction

can be predicted in thermodynamics and kinetic using the free energy change and the activation energy, respectively.

According to the transition-state theory, the intermediate formed between reactant (initial state) and product (final state) for any reaction path is known as the transition state with the highest potential energy. For the coke dimerization, the initial state and the final state were represented by diatomic and dimer coke adsorbed on the surface, while the transition state was figured out and confirmed by the one imaginary frequency consideration. The minimum energy path of coke dimerization on the γ-Al_2O_3 surface is illustrated in Figure 16.

In thermodynamics, the free energy change is used to describe whether the reaction occurs spontaneously. At the ground state condition (T= 0 K), the free energy change of coke dimerization on the γ-Al_2O_3 surface is -5.36 eV. This result indicates that the coke dimerization is a spontaneous reaction. However, when also considered in the liquid phase reaction operated in the temperature range of 373 K to 773 K, the free energy change is no different from the ground state condition. Thus, it points out that the coke dimerization remains spontaneously on the γ-Al_2O_3 surface during the aqueous phase reaction. In the kinetic consideration, the activation energy is the minimum energy required for a reaction to proceed forward calculated by the energy difference between the initial and the transition state. The activation energy barrier for this reaction is 1.89 eV. The required energy for the dimerization is too high resulting from this investigation was performed in low coverage of coke. However, once the coke coverage is high enough to the adsorbed coke reach in adjacent sites, the dimerization is encouraged, as mentioned in the adsorption section.

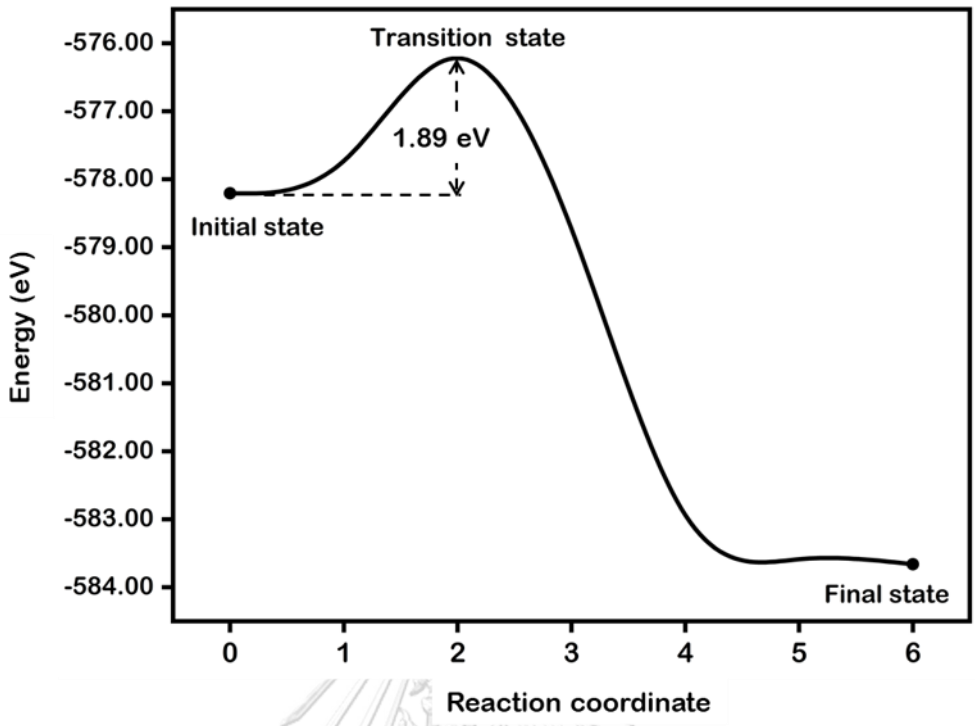

Figure 16 The coke dimerization path on the γ-Al_2O_3 surfaceusing the Climbing image-nudged elastic band (CI-NEB) method

4.2 Effect of water coverage on coke behaviour

During the aqueous phase reaction, the modification of γ-Al_2O_3 surface via water-surface interaction is unavoidable. Therefore, the effect of water coverage on coke behavior was investigated. Herein, the model structure of the γ-Al_2O_3 surface was modified based on partial hydroxylated and full hydroxylated models. For the partial hydroxylated γ-Al_2O_3 surface (OH/γ-Al_2O_3), the explicit solvent of four water molecules is added that the most stable geometry of OH/γ-Al_2O_3(110) is revealed in Figure 9. For the fully hydroxylated γ-Al_2O_3 surface, the surface model of γ-AlOOH(010) representing γ-Al_2O_3 surface with saturated water leading to phase transformation is selected, as shown in Figure 10. For the coke formation process, the reaction pathway starts from coke initiation of C_1-atomic adsorption on catalyst surface before dimerization of coke forming C_2-dimer. Then, coke polymerization is taken place by the formation of the higher coke represented by the C_6-cyclic.

4.2.1 Coke adsorption on the partial and fully hydroxylated surface

In this section, the coke adsorption, including C_1-atomic, C_2-dimer, and C_6-cyclic on OH/γ-Al_2O_3(110) and γ-AlOOH(010) surfaces were investigated as demonstrated in Figure 17, and the E_{ads} are summarized in Table 4.

For the partially hydrated surface (OH/γ-Al_2O_3), the C_1-atomic and C_2-dimer prefer to adsorb on the oxygen site labeled as O(1)' of OH/γ-Al_2O_3 surface with the E_{ads} of -3.34 eV and -4.72 eV. At the same time, the C_6-cyclic is adsorbed on the oxygen site labeled as O(1) on OH/γ-Al_2O_3 surface with the E_{ads} of -2.53 eV. Hydroxylation of γ-Al_2O_3(110) surface creates adsorbed species of water (H_2O), hydroxyl group (OH), and detached hydrogen (H) along the OH/γ-Al_2O_3 surface. These adsorbed species are closed by the O(1) site, which is usually active for coke adsorption on γ-Al_2O_3 surface. The presence of H_2O and OH species adsorption makes the O(1) site more difficult to access. Hence, the active site for coke formation is moved to O(1)' which is less active than O(1) leading to lower E_{ads} than γ-Al_2O_3(110) surface.

For the fully hydrated surface (γ-AlOOH), all types of coke prefer to adsorb on the O1'' of OH site of the γ-AlOOH surface. The C_1-atomic and C_2-dimer were adsorbed with the E_{ads} of -1.72 eV and -3.55 eV, respectively. Moreover, the enlargement of higher cokes as C_6-cyclic decreases the E_{ads} into -1.59 eV, which refers to the weakening of interaction between a higher coke and γ-AlOOH surface. These results suggest that full hydroxylation of γ-Al_2O_3 until phase transformation to γ-AlOOH obviously exhibits a decrease in the interaction between coke and γ-Al_2O_3 surface because the OH group, which is an inactive species, is presented entirely on the top layer of γ-AlOOH(110) surface diminishing the interaction between coke and surface. Furthermore, the larger site of higher cokes in cyclic form increases the steric effect reduces the coke-surface interaction. Therefore, the interaction between γ-AlOOH(110) surface and all cokes is the weakest.

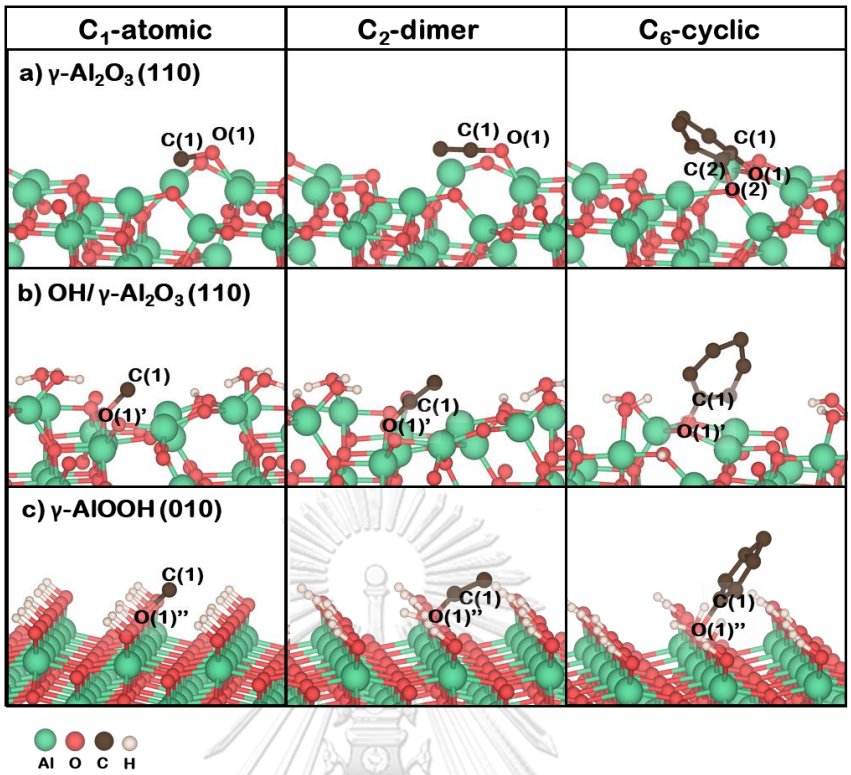

Figure 17 The most stable configuration of coke C_1-atomic, C_2-dimer, and C_6-cyclic on γ-Al_2O_3 (110), OH/γ-Al_2O_3 (110), and γ-AlOOH (010).Table 4 Adsorption energy of various types of coke on the γ-Al_2O_3 (110), OH/γ-Al_2O_3 (110), and γ-AlOOH (010) surface.

Coke form	The adsorption energy(eV)		
	γ-Al_2O_3(110)	OH/ γ-Al_2O_3(110)	γ-AlOOH(010)
C_1-atomic	-3.86	-3.34	-1.72
C_2-dimer	-5.89	-4.72	-3.55
C_6-cyclic	-4.50	-2.53	-1.59

4.2.2 Coke evolution on the partial and fully hydroxylated surface

The LH mechanism was applied to elucidate the influence of water coverage on γ-Al_2O_3(110), which usually occurs in the aqueous phase reaction, on coke evolution through continuous growth. The elementary step and the formation energy calculation for the continuous growth of coke are following in the previous section. The relative ΔE_{form} diagram for the continuous growth of coke along OH/γ-Al_2O_3(110) and γ-

AlOOH(010) surfaces comparing to γ-Al_2O_3(110) surfaces are plotted as expressed in Figure 18. The relative ΔE_{form} of coke evolution is reported in Table 5.

The coke initiation of C_1-atomic adsorption can be taken place on OH/γ-Al_2O_3(110), and γ-AlOOH(010) surfaces with the E_{ads} of -3.34 and -1.72 eV, respectively. After that, coke evolution is started with coke dimerization forming C_2-dimer. The relative ΔE_{form} of C_2-dimer are -8.37 eV and -8.31 eV for OH/γ-Al_2O_3(110) and γ-AlOOH(010) surface. Finally, the cyclic aromatic structure of C_6-cyclic is formed with the relative ΔE_{form} of -21.26 eV and -28.79 eV on OH/γ-Al_2O_3(110) and γ-AlOOH(010) surfaces, respectively.

Hydroxylation of γ-Al_2O_3(110) including partial hydroxylation to form OH/γ-Al_2O_3(110) surface and complete hydroxylation to form γ-AlOOH(010) surface weakens an interaction between C(1) and C(2) to perform the C_2-dimer, implying resistance of coke initiation as well as retarding coke agglomeration of C_2-dimer formation. However, the presence of the OH group on hydroxylated γ-Al_2O_3(110) surfaces promotes coke cyclization, enhancing graphitic coke formation on the hydroxylated surface. Moreover, the increase in the OH group also raises the production of C_6-cyclic formation observed by the more negative value of relative ΔE_{form} comparing to γ-Al_2O_3(110) surface.

Table 5 The relative ΔE_{form} of coke evolution along the γ-Al_2O_3 (110), OH/γ-Al_2O_3 (110), and γ-AlOOH (010) surface.

จุฬาลงกรณ์มหาวิทยาลัย
CHULALONGKORN UNIVERSITY

Step	**Reaction pathway**	**The relative ΔE_{form} (eV)**		
		γ-Al_2O_3	**OH/ γ-Al_2O_3**	**γ-AlOOH**
(a)	C_1 atomic on clean surface	-3.86	-3.34	-1.72
(b)	C_1 atomic to C_2 dimer	-9.02	-8.34	-8.49
(c)	C_2 dimer to C_6 cyclic	-21.01	-21.59	-28.96

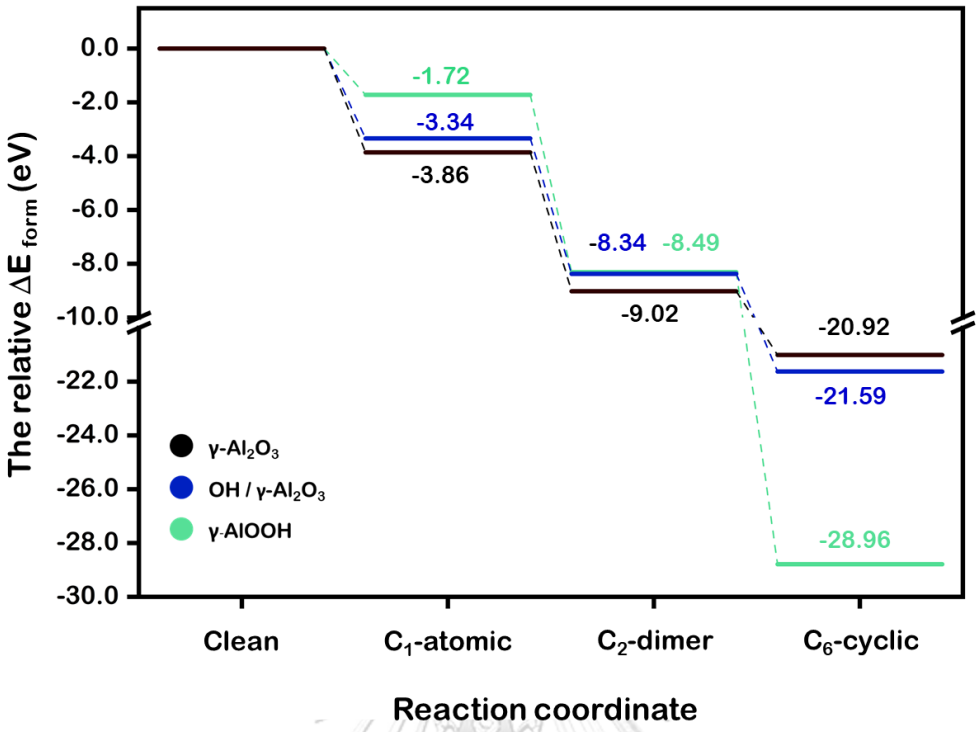

Figure 18 The relative ΔE_{form} diagram for the coke evolution on γ-Al_2O_3, OH/γ-Al_2O_3, and γ-AlOOH surface based on the LH mechanism.

4.2.3 The Electronic properties

To provide insight into the interaction between cokes and the surface, the Bader charge analysis and charge density difference were performed. The charge density differences presenting the number of contact points between coke and each substrate during the adsorption process are displayed in Figure 19. The charge accumulation and depletion are represented by yellow and violet regions, respectively. In addition, the Bader charge changes of the adsorbed cokes, including C_1-atomic, C_2-dimer, and C_6-cyclic on each surface of γ-Al_2O_3 (110), OH/ γ-Al_2O_3(110), and γ-AlOOH(010) are shown in Table 6. The negative and positive signs represent electron gain and loss, respectively.

For γ-Al_2O_3(110) surface, the C_1-atomic was adsorbed, creating one contact point between C_1-atomic and O(1). The small Bader charge change between coke and surface around ±0.05 |*e*| implies that this Bader charge result is controversial. However, considering the O(1) atom, which connects to C_1-atomic, demonstrated the positive value of +0.33 |*e*|, indicating the role of the electron donor of O(1) during the coke

initiation process. Propagation of coke after adsorption of C_1-atomic obviously reveals electron transfer from γ-Al_2O_3(110) surface to adsorbed coke via O(1) bridge that the evolution of cyclic higher coke decreases the amount of electron donation from γ-Al_2O_3(110) surface.

For all hydroxylated surfaces, the C_1-atomic create a single contact point to O(1)' and O(1)" sites of OH/γ-Al_2O_3(110) and γ-AlOOH(010), respectively. All Bader charge changes of contacted O site reveal a positive value, for example, the +0.23 |*e*| for O(1)' and +0.15 |*e*| for O(1)" together with the negative value of adsorbed C_1-atomic (denoted as -0.18 |*e*| for OH/γ-Al_2O_3(110) and γ-AlOOH(010) surfaces) indicate the electron transfer from substrate to adsorbed coke which plays as an electron acceptor role during the adsorption process. For the evolution of higher coke, the adsorbed coke remains an electron acceptor while an electron is donated from the surface. Focusing on the O site bonded with adsorbed coke (defined as O(1), O(1)', and (O)1" on γ-Al_2O_3(110), OH/γ-Al_2O_3(110), and γ-AlOOH(010) surfaces, respectively), amount of electron loss from O site during coke adsorption process accords to the interaction between substrate and cokes. Hydroxylation of γ-Al_2O_3 limits electron donation from surface to adsorbed coke in order: γ-Al_2O_3 > OH/ γ-Al_2O_3 > γ-AlOOH making the coke-substrates interaction weaken. These results are in good agreement with the lower E_{ads} value of cokes on hydroxylated surfaces of OH/ γ-Al_2O_3 and γ-AlOOH comparing with γ-Al_2O_3 surface.

จุฬาลงกรณ์มหาวิทยาลัย
CHULALONGKORN UNIVERSITY

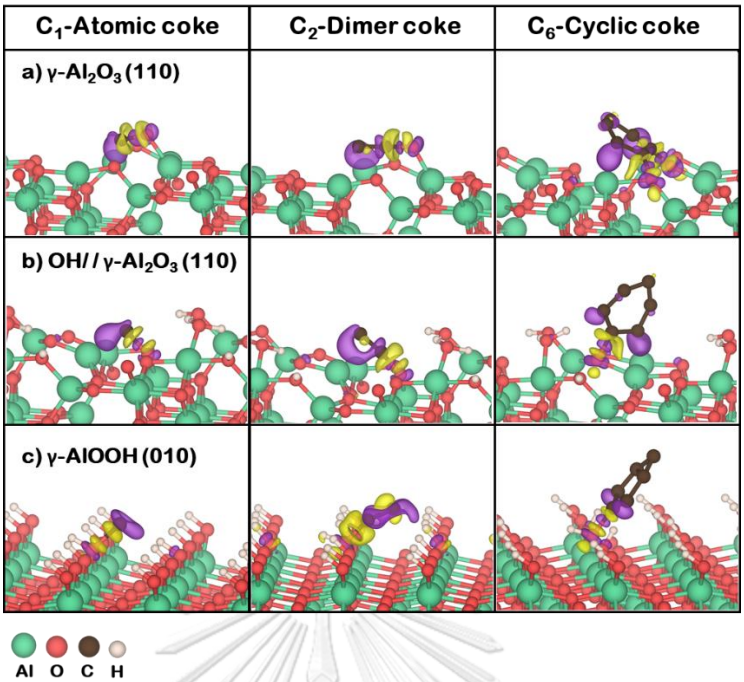

Figure 19 Charge density differences of coke adsorption on (a) the γ-Al_2O_3, (b) the OH/ γ-Al_2O_3, and (c) the γ-AlOOH surfacewith isovalue of ±0.015 e $Å^{-3}$. The violet region for electron depletion and yellow for electron accumulation.

Table 6 Bader charge change of each component for coke adsorption on γ-Al_2O_3, OH/ γ-Al_2O_3, and γ-AlOOH surface.

surface	Component	The Bader charge change (|*e*|)		
		C_1-atomic	C_2-dimer	C_6-cyclic
γ-Al_2O_3	surface	-0.05	+0.24	+0.34
	adsorbate	+0.05	-0.24	-0.34
	oxygen atom	+0.33	+0.26	+0.33
OH/ γ-Al_2O_3	surface	+0.18	+0.29	+0.28
	adsorbate	-0.18	-0.29	-0.28
	oxygen atom	+0.23	+0.25	+0.24
γ-AlOOH	surface	+0.18	+0.16	+0.20
	adsorbate	-0.18	-0.16	-0.20
	oxygen atom	+0.15	+0.13	+0.19

4.3 Effect of oxygen vacancy on coke behavior

In the actual condition, the oxygen vacancy has a chance to be found in the synthesized metal oxide. The oxygen vacancy contribution can tailor the metal oxide's essential properties, e.g., change catalytic reactivity and the reaction pathways.[23,24,49] For this reason, the role of oxygen vacancy on deactivation by coking has gained attention and explored through the coke behavior on the oxygen vacancy surface. The oxygen vacancy surface was performed by removing the oxygen atom on the γ-Al_2O_3 surface and then adding the water molecule similar to OH/γ-Al_2O_3. The most stable configuration of the oxygen vacancy surface (O_v/OH/γ-Al_2O_3) is shown in Figure 20.

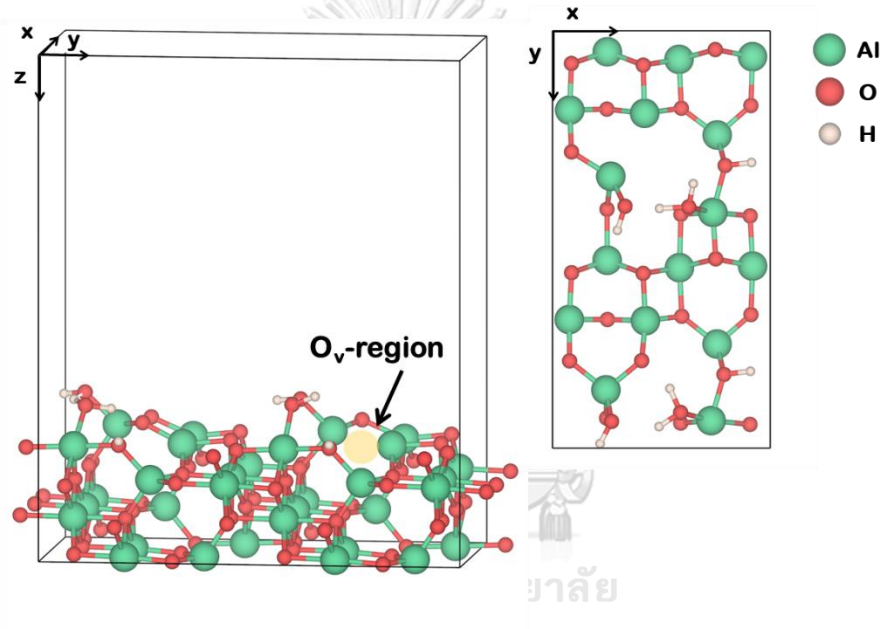

Figure 20 The most stable configuration of the O_v/ OH/ γ-Al_2O_3 surface

4.3.1 Coke adsorption on the oxygen vacancy surface

The coke adsorption was investigated in O_v/OH/γ-Al_2O_3 surfaces to understand the interaction between coke and the O_v/OH/γ-Al_2O_3 surface. The adsorbed coke consists of C_1-atomic, C_2-dimer coke, and C_6-cyclic. The most stable configurations of adsorbed coke on the O_v/OH/γ-Al_2O_3 surface are shown in Figure 21, and the adsorption energy is reported in

Table *7*. The oxygen vacancy region (O_v-region) has become a new active site in the adsorption process for all adsorbed coke. The E_{ads} are -5.51 eV, -8.80 eV, and -5.78 eV for C_1-atomic, C_2-dimer and C_6-cyclic. This result indicates that their coke has

strong interaction with the O_v/OH/γ-Al_2O_3 surface. However, the C_6-cyclic, a larger coke form, is less negative adsorption energy than the C_2-dimer resulting from the steric hindrance of the coke and the presence of the OH group covered on the surface. Compared with the OH/γ-Al_2O_3 surface, the E_{ads} has noticeably increased for the oxygen vacancy surface, particularly after dimerization. Moreover, the adsorbed coke also led to the surface reconstruction in terms of the enlargement of the O_v-region, and the higher coke also gives more reconstruction. These observations point out the highly negative value of adsorption energy could be attributed to the reconstruction at O_v-surface.

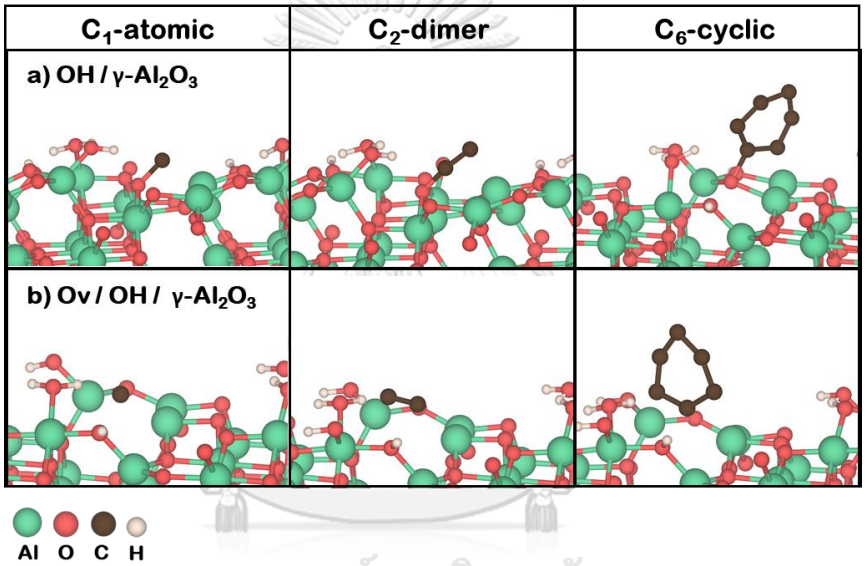

Figure 21 The favorable adsorption of C_1-atomic, C_2-dimer, and C_6-cyclic on OH/γ-Al_2O_3 (110) and O_v/OH/ γ-Al_2O_3 (110).

Table 7 Adsorption energy of coke adsorption on OH/ γ-Al_2O_3 and O_v/OH/ γ-Al_2O_3 surface.

Coke form	**The E_{ads} (eV)**	
	OH/ γ-Al_2O_3	**O_v/OH/ γ-Al_2O_3**
C_1-atomic	-3.34	-5.51
C_2-dimer	-4.72	-8.80
C_6-cyclic	-2.53	-5.78

4.3.2 Coke evolution on the oxygen vacancy surface

The continuous growth of coke is examined on the oxygen vacancy surface based on the LH mechanism. The relative ΔE_{form} of adsorbed coke is reported in Table 8, while the relative ΔE_{form} diagram comparing with γ-Al_2O_3(110) surfaces are shown in Figure 22. The relative ΔE_{form} are -5.51 eV, -10.27 eV, and -14.00 eV for C_1-atomic, C_2-dimer, and C_6-cyclic coke. The negative value of ΔE_{form} indicated that their step is energetically favorable to proceed forward. The increase in the magnitude of relative ΔE_{form} when the number of carbon atoms increased implies that the probability of the coke evolution pathway grows from atomic to larger coke on O_v/OH/γ-Al_2O_3 surface, similar to OH/γ-Al_2O_3 surface.

For the coke initiation, the formation of C_1-atomic and C_2-dimer is promoted on the O_v/OH/γ-Al_2O_3 comparing with the OH/γ-Al_2O_3 surface. On the contrary, the C_6-cyclic is more difficult to form on the O_v/OH/γ-Al_2O_3 due to strengthening interaction between coke and surface. Therefore, this result implies that the existence of oxygen vacancy suppresses the coke evolution to higher coke.

Table 8 The relative formation energy of coke on OH/γ-Al_2O_3 (110), and O_v/OH/γ-Al_2O_3 surface.

จุฬาลงกรณ์มหาวิทยาลัย
Chulalongkorn University

Step	Reaction pathway	The relative formation energy (eV)	
		OH/ γ-Al_2O_3	O_v/OH/ γ-Al_2O_3
(a)	C_1 atomic on clean surface	-3.34	-5.51
(b)	C_1 atomic to C_2 dimer	-8.34	-10.27
(c)	C_2 dimer to C_6 cyclic	-21.59	-14.00

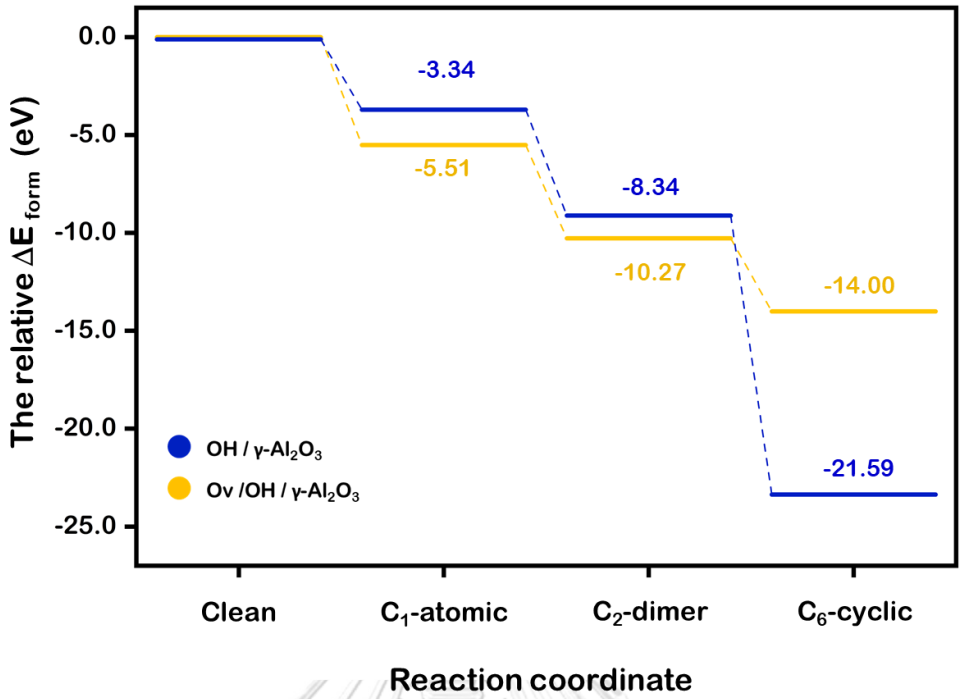

Figure 22 The relative ΔE_{form} diagram for the coke evolution on the OH/γ-Al_2O_3 (110) and O_v/OH/γ-Al_2O_3 (110) surface based on LH mechanism

4.3.2 The Electronic properties

The Bader charge analysis was investigated based on Bader charge analysis for describing the coke behavior on the oxygen vacancy surface. The Bader charge changes between the adsorbed coke and the surface are given in Table 9. The negative and positive signs represent electron gain and loss, respectively. Moreover, the charge density difference of each configuration was performed and shown in Figure 23. The electron accumulation and depletion are labeled in yellow and violet regions.

The adsorbed coke interacts with the O_v/OH/γ-Al_2O_3 surface as an electron acceptor, similar to OH/γ-Al_2O_3 surface. For the OH/γ-Al_2O_3 surface, the gaining electron of C_1-atomic, C_2-diatomic, C_2-dimer coke, and C_6-cyclic are -0.18|*e*|, -0.35|*e*|, -0.29|*e*|, and -0.28|e|. For the O_v/OH/γ-Al_2O_3 surface, the gaining electron of C_1-atomic, C_2-diatomic, C_2-dimer coke, and C_6-cyclic are -1.44|*e*|, -1.63|*e*|, -1.51|*e*|, and -1.55|*e*|, respectively. Compared with the OH/ γ-Al_2O_3 surface, the electron exchange between adsorbed coke and surface dramatically increases as the oxygen vacancy was formed

on the surface. These results confirm that the coke-surface interaction on the O_v/OH/γ-Al_2O_3 is stronger than the OH/γ-Al_2O_3 surface, in agreement with the adsorption energy.

Table 9 The Bader charge change of each component for coke adsorption on OH/γ-Al_2O_3 (110) and O_v/OH/γ-Al_2O_3 (110) surface.

surface	Component	C_1 -atomic	C_2-dimer	C_6-cyclic
OH/ γ-Al_2O_3	surface	+0.18	+0.29	+0.28
	adsorbate	-0.18	-0.29	-0.28
Ov/OH/ γ-Al_2O_3	surface	+1.44	+1.51	+1.55
	adsorbate	-1.44	-1.51	-1.55

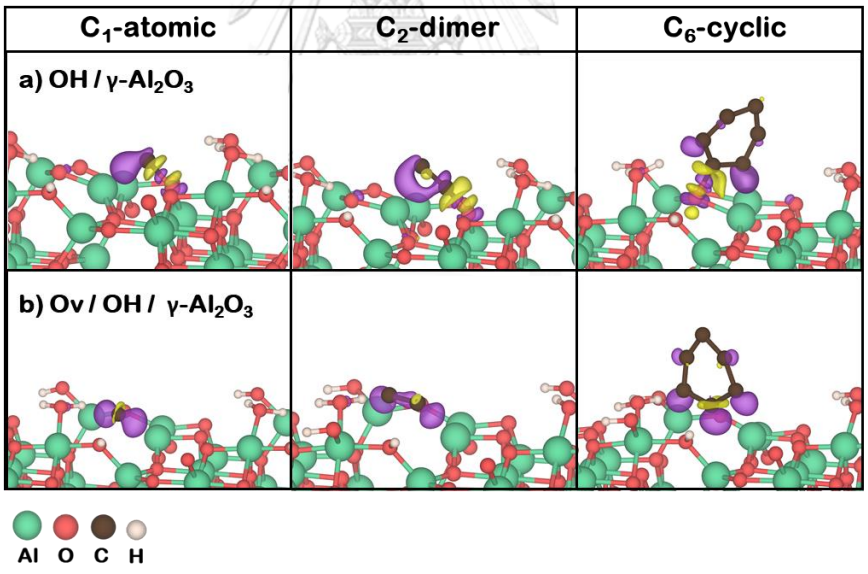

Figure 23 Charge density differences of coke adsorption on (a) OH/γ-Al_2O_3 and (b) O_v/OH/γ-Al_2O_3 surface with isovalue of ±0.015 e $Å^{-3}$. The violet region for electron depletion and yellow for electron accumulation.

4.4 Effect of temperature

Having determined the coke behavior through the coke adsorption, the thermodynamics consideration can be applied to describe the coke behavior as a function of the temperature. In this section, the considered temperatures are in the range of 373-773 K to comply with the aqueous phase reaction.

The free energy change of coke adsorption (ΔG_{ads}) was calculated using the vibrational analysis. The ΔG_{ads} profiles of γ-Al_2O_3, OH/γ-Al_2O_3, and γ-AlOOH surface are illustrated in Figure 24. At ground state condition (T= 0 K), The ΔG_{ads} was corrected by the ΔZPE term only. It found that ΔG_{ads} of coke adsorption decreased in order: γ-Al_2O_3 > OH/γ-Al_2O_3 > γ-AlOOH, in agreement with adsorption strength. At the given temperature, the ΔG_{ads} is also contributed by the thermal correction in terms of the partition function from the vibration of adsorbed coke. For all surfaces, the ΔG_{ads} of coke tends to decrease when the temperature increase. It implies that an increase in temperature leads to the weakening of adsorption strength. Moreover, the result has a similar trend for O_v/OH/γ-Al_2O_3 surface.

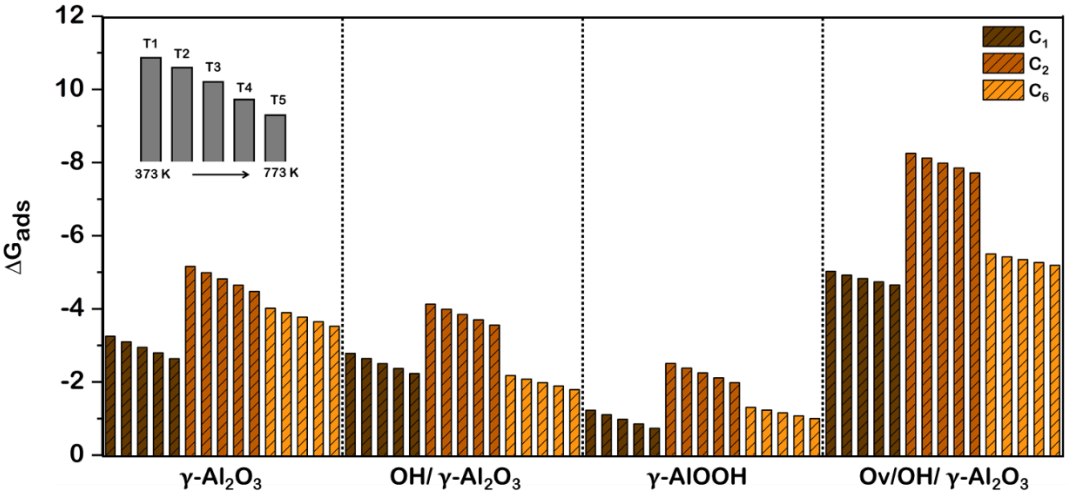

Figure 24 The ΔG_{ads} profiles of γ-Al_2O_3(110), OH/γ-Al_2O_3(110), γ-AlOOH(010), and Ov/OH/γ-Al_2O_3(110) surface in the temperatures of 373 - 773 K

CHAPTER 5
CONCLUSION

The DFT calculations have been performed to investigate the coke behavior on the γ-Al_2O_3 based catalyst. The result exposes that the coke formation on the γ-Al_2O_3 can be divided into three steps: coke initiation, dimerization, and polymerization. During the initiation stage, the atomic coke is strongly chemisorbed on the γ-Al_2O_3 surface. In the dimerization stage, the two-atomic coke is preferable to transform into a dimer form. Lastly, the coke polymerization generated higher coke with more energetically favorable. The polymerization forming higher coke prefers a cyclic form of coke to the aliphatic one due to its less steric effect. Therefore, the cyclic coke formed is more difficult to be removed than that of the aliphatic coke, promoting higher deactivation, although they consisted of the same number of carbons in the molecule. Furthermore, the feasibility of coke evolution is approximately determined by the coke dimerization, the simplest route to the continuous growth of coke. Both thermodynamic and kinetic considerations evidence that the coke dimerization is spontaneous and exothermic with the energy barrier of 1.89 eV to proceed forward. For the water coverage effect on coke behavior, all coke adsorption strength was reduced in the order: γ-Al_2O_3 > OH/ γ-Al_2O_3 > γ-AlOOH. The Bader charge analysis further reveals that the adsorbed coke plays as the electron acceptor from the surfaces. The electron exchange of the oxygen atom being considered active sites for coke adsorption also confirmed the increasing water coverage weakened the interaction between coke and surface, the hydroxylated surface retard the coke formation on γ-Al_2O_3. Although the coke-surface interaction is weakened on the hydroxylated surface, the coke polymerization is encouraged, considering the formation energy of coke evolution. For the effect of oxygen vacancy on coke behavior, the adsorption strength of coke is significantly increased over the oxygen vacancy surface. Moreover, the charge transfer between coke and the surface is higher than the perfect surface without oxygen vacancy. Thus, oxygen vacancy may promote coke formation and result in the coke elimination from the γ-Al_2O_3 based catalyst more difficult.

จุฬาลงกรณ์มหาวิทยาลัย
CHULALONGKORN UNIVERSITY

REFERENCES

1 Coronado, I. *et al.* A review of catalytic aqueous-phase reforming of oxygenated hydrocarbons derived from biorefinery water fractions. *International Journal of Hydrogen Energy* **41**, 11003-11032, doi:10.1016/j.ijhydene.2016.05.032 (2016).

2 Guo, Y., Azmat, M. U., Liu, X., Wang, Y. & Lu, G. Effect of support's basic properties on hydrogen production in aqueous-phase reforming of glycerol and correlation between WGS and APR. *Applied Energy* **92**, 218-223, doi:10.1016/j.apenergy.2011.10.020 (2012).

3 Dosso, L. A., Vera, C. R. & Grau, J. M. Aqueous phase reforming of polyols from glucose degradation by reaction over Pt/alumina catalysts modified by Ni or Co. *International Journal of Hydrogen Energy* **42**, 18853-18864, doi:10.1016/j.ijhydene.2017.06.100 (2017).

4 Duarte, H. A., Sad, M. E. & Apesteguía, C. R. Bio-hydrogen production by APR of C 2 -C 6 polyols on Pt/Al 2 O 3 : Dependence of H 2 productivity on metal content. *Catalysis Today* **296**, 59-65, doi:10.1016/j.cattod.2017.04.067 (2017).

5 Soszka, E., Jędrzejczyk, M., Kocemba, I., Keller, N. & Ruppert, A. Ni-Pd/γ-Al2O3 Catalysts in the Hydrogenation of Levulinic Acid and Hydroxymethylfurfural towards Value Added Chemicals. *Catalysts* **10**, doi:10.3390/catal10091026 (2020).

6 Yamaguchi, S. *et al.* Catalytic Conversion of Biomass-Derived Carbohydrates to Methyl Lactate by Acid–Base Bifunctional γ-Al2O3. *ACS Sustainable Chemistry & Engineering* **6**, 8113-8117, doi:10.1021/acssuschemeng.8b00809 (2018).

7 El Doukkali, M. *et al.* Deactivation study of the Pt and/or Ni-based γ-Al2O3 catalysts used in the aqueous phase reforming of glycerol for H2 production. *Applied Catalysis A: General* **472**, 80-91, doi:10.1016/j.apcata.2013.12.015 (2014).

8 Jang, E. J., Lee, J. & Kwak, J. H. Morphology change and phase transformation of alumina related to defect sites and its use in catalyst preparation. *Catalysis Today* **352**, 323-328.

9 Rinaldi, R., Fujiwara, F. & Schuchardt, U. Chemical and physical changes related to the deactivation of alumina used in catalytic epoxidation with hydrogen peroxide. *Journal of Catalysis* **245**, 456-465.

10 Ravenelle, R. M., Copeland, J. R., Kim, W.-G., Crittenden, J. C. & Sievers, C. Structural Changes of γ-Al2O3-Supported Catalysts in Hot Liquid Water. *ACS Catalysis* **1**, 552-561.

11 Sádaba, I., López Granados, M., Riisager, A. & Taarning, E. Deactivation of solid catalysts in liquid media: the case of leaching of active sites in biomass conversion reactions. *Green Chemistry* **17**, 4133-4145.

12 Matsushita, K., Hauser, A., Marafi, A., Koide, R. & Stanislaus, A. Initial coke deposition on hydrotreating catalysts. Part 1. Changes in coke properties as a function of time on stream. *Fuel* **83**, 1031-1038, doi:10.1016/j.fuel.2003.10.015 (2004).

13 Lei, N. *et al.* Understanding the deactivation behavior of Pt/WO3/Al2O3 catalyst in the glycerol hydrogenolysis reaction. *Chinese Journal of Catalysis* **41**, 1261-1267, doi:10.1016/s1872-2067(20)63549-5 (2020).

จุฬาลงกรณ์มหาวิทยาลัย
CHULALONGKORN UNIVERSITY

14 Abi Aad, J. *et al.* Chemical Weathering of Alumina in Aqueous Suspension at Ambient Pressure: A Mechanistic Study. *ChemCatChem* **9**, 2186-2194, doi:10.1002/cctc.201700145 (2017).

15 Argyle, M. & Bartholomew, C. Heterogeneous Catalyst Deactivation and Regeneration: A Review. *Catalysts* **5**, 145-269, doi:10.3390/catal5010145 (2015).

16 Ruiz Puigdollers, A., Schlexer, P., Tosoni, S. & Pacchioni, G. Increasing Oxide Reducibility: The Role of Metal/Oxide Interfaces in the Formation of Oxygen Vacancies. *ACS Catalysis* **7**, 6493-6513, doi:10.1021/acscatal.7b01913 (2017).

17 Yazdanmehr, M., Jalali-Asadabadi, S., Nematollahi, J., Nourmohammadi, A. & Ahmad, I. Predictions of bandgap and subbands of γ−Al2O3 in presence of intrinsic point defects by DFT+TB-mBJ. *Computational Condensed Matter* **19**, doi:10.1016/j.cocom.2019.e00379 (2019).

18 Peterson, E. J. *et al.* Low-temperature carbon monoxide oxidation catalysed by regenerable atomically dispersed palladium on alumina. *Nat Commun* **5**, 4885, doi:10.1038/ncomms5885 (2014).

19 Li, X., Zhang, L., Wang, S. & Wu, Y. Recent Advances in Aqueous-Phase Catalytic Conversions of Biomass Platform Chemicals Over Heterogeneous Catalysts. *Front Chem* **7**, 948, doi:10.3389/fchem.2019.00948 (2019).

20 Chheda, J. N., Huber, G. W. & Dumesic, J. A. Liquid-phase catalytic processing of biomass-derived oxygenated hydrocarbons to fuels and chemicals. *Angew Chem Int Ed Engl* **46**, 7164-7183, doi:10.1002/anie.200604274 (2007).

21 Ochoa, A., Bilbao, J., Gayubo, A. G. & Castaño, P. Coke formation and deactivation during catalytic reforming of biomass and waste pyrolysis products: A review. *Renewable and Sustainable Energy Reviews* **119**, doi:10.1016/j.rser.2019.109600 (2020).

22 Reocreux, R. *et al.* Reactivity of shape-controlled crystals and metadynamics simulations locate the weak spots of alumina in water. *Nat Commun* **10**, 3139, doi:10.1038/s41467-019-10981-9 (2019).

23 Wang, L. *et al.* Oxygen vacancy clusters essential for the catalytic activity of CeO2 nanocubes for o-xylene oxidation. *Sci Rep* **7**, 12845, doi:10.1038/s41598-017-13178-6 (2017).

24 Ye, J., Liu, C., Mei, D. & Ge, Q. Active Oxygen Vacancy Site for Methanol Synthesis from CO2 Hydrogenation on In2O3(110): A DFT Study. *ACS Catalysis* **3**, 1296-1306, doi:10.1021/cs400132a (2013).

25 Widmann, D. & Behm, R. J. Activation of molecular oxygen and the nature of the active oxygen species for CO oxidation on oxide supported Au catalysts. *Accounts of chemical research* **47**, 740-749 (2014).

26 Hinuma, Y. *et al.* Density Functional Theory Calculations of Oxygen Vacancy Formation and Subsequent Molecular Adsorption on Oxide Surfaces. *The Journal of Physical Chemistry C* **122**, 29435-29444, doi:10.1021/acs.jpcc.8b11279 (2018).

27 Dang, Y., Liu, Y., Feng, X., Chen, X. & Yang, C. Effect of dispersion on the adsorption of polycyclic aromatic hydrocarbons over the γ-Al2O3 (110) surface. *Applied Surface Science* **486**, 137-143, doi:10.1016/j.apsusc.2019.05.020 (2019).

28 Krokidis, X. *et al.* Theoretical study of the dehydration process of boehmite to γ-alumina. *The Journal of Physical Chemistry B* **105**, 5121-5130 (2001).

29 Demichelis, R., Noël, Y., Ugliengo, P., Zicovich-Wilson, C. M. & Dovesi, R. Physico-Chemical Features of Aluminum Hydroxides As Modeled with the Hybrid B3LYP Functional and Localized Basis Functions. *The Journal of Physical Chemistry C* **115**, 13107-13134, doi:10.1021/jp200523x (2011).

30 Noel, Y. *et al.* Ab initio quantum mechanical study of γ-AlOOH boehmite: structure and vibrational spectrum. *Physics and Chemistry of Minerals* **36**, 47-59, doi:10.1007/s00269-008-0257-z (2008).

31 Raybaud, P. *et al.* Morphology and surface properties of boehmite (γ-AlOOH): a density functional theory study. *Journal of Catalysis* **201**, 236-246 (2001).

32 Kohn, W. & Sham, L. J. Self-Consistent Equations Including Exchange and Correlation Effects. *Physical Review* **140**, A1133-A1138, doi:10.1103/PhysRev.140.A1133 (1965).

33 Kresse, G. & Hafner, J. Ab initio molecular dynamics for liquid metals. *Phys Rev B Condens Matter* **47**, 558-561, doi:10.1103/physrevb.47.558 (1993).

34 Kresse, G. & Furthmüller, J. Efficient iterative schemes for ab initio total-energy calculations using a plane-wave basis set. *Physical review B* **54**, 11169 (1996).

35 Blochl, P. E. Projector augmented-wave method. *Phys Rev B Condens Matter* **50**, 17953-17979, doi:10.1103/physrevb.50.17953 (1994).

36 Kresse, G. & Joubert, D. From ultrasoft pseudopotentials to the projector augmented-wave method. *Physical review b* **59**, 1758 (1999).

37 Perdew, J. P., Burke, K. & Ernzerhof, M. Generalized gradient approximation made simple. *Physical review letters* **77**, 3865 (1996).

38 Grimme, S., Antony, J., Ehrlich, S. & Krieg, H. A consistent and accurate ab initio parametrization of density functional dispersion correction (DFT-D) for the 94 elements H-Pu. *J Chem Phys* **132**, 154104, doi:10.1063/1.3382344 (2010).

39 Monkhorst, H. J. & Pack, J. D. Special points for Brillouin-zone integrations. *Physical Review B* **13**, 5188-5192, doi:10.1103/PhysRevB.13.5188 (1976).

40 Teter, M. P., Payne, M. C. & Allan, D. C. Solution of Schrodinger's equation for large systems. *Phys Rev B Condens Matter* **40**, 12255-12263, doi:10.1103/physrevb.40.12255 (1989).

41 Fu, C. L. & Ho, K. M. First-principles calculation of the equilibrium ground-state properties of transition metals: Applications to Nb and Mo. *Physical Review B* **28**, 5480-5486, doi:10.1103/PhysRevB.28.5480 (1983).

42 Henkelman, G., Arnaldsson, A. & Jónsson, H. A fast and robust algorithm for Bader decomposition of charge density. *Computational Materials Science* **36**, 354-360, doi:10.1016/j.commatsci.2005.04.010 (2006).

43 Tang, W., Sanville, E. & Henkelman, G. A grid-based Bader analysis algorithm without lattice bias. *J Phys Condens Matter* **21**, 084204, doi:10.1088/0953-8984/21/8/084204 (2009).

44 Digne, M., Sautet, P., Raybaud, P., Euzen, P. & Toulhoat, H. Hydroxyl groups on γ-alumina surfaces: a DFT study. *Journal of Catalysis* **211**, 1-5 (2002).

45 Digne, M. Use of DFT to achieve a rational understanding of acid?basic properties of ?-alumina surfaces. *Journal of Catalysis* **226**, 54-68, doi:10.1016/j.jcat.2004.04.020 (2004).

46 Tan, K., Dixit, M., Dean, J. & Mpourmpakis, G. Predicting Metal–Support Interactions in Oxide-Supported Single-Atom Catalysts. *Industrial & Engineering Chemistry Research* **58**, 20236-20246, doi:10.1021/acs.iecr.9b04068 (2019).

47 Wischert, R., Coperet, C., Delbecq, F. & Sautet, P. Optimal water coverage on alumina: a key to generate Lewis acid-base pairs that are reactive towards the C-H bond activation of methane. *Angew Chem Int Ed Engl* **50**, 3202-3205, doi:10.1002/anie.201006794 (2011).

48 Wischert, R., Laurent, P., Coperet, C., Delbecq, F. & Sautet, P. gamma-Alumina: the essential and unexpected role of water for the structure, stability, and reactivity of "defect" sites. *J Am Chem Soc* **134**, 14430-14449, doi:10.1021/ja3042383 (2012).

49 Zhang, Y.-C. *et al.* Role of oxygen vacancies in photocatalytic water oxidation on ceria oxide: Experiment and DFT studies. *Applied Catalysis B: Environmental* **224**, 101-108, doi:10.1016/j.apcatb.2017.10.049 (2018).

จุฬาลงกรณ์มหาวิทยาลัย
CHULALONGKORN UNIVERSITY

จุฬาลงกรณ์มหาวิทยาลัย
Chulalongkorn University

VITA

NAME	Phakaorn Aphichoksiri
DATE OF BIRTH	12 September 1994
PLACE OF BIRTH	Nakhon Pathom

จุฬาลงกรณ์มหาวิทยาลัย
CHULALONGKORN UNIVERSITY